2008

Experimental Investigation of Unsaturated Soil Stiffness

Ananth Bukkapatnam Tirumala
Louisiana State University and Agricultural and Mechanical College, abukka1@lsu.edu

EXPERIMENTAL INVESTIGATION OF UNSATURATED SOIL STIFFNESS

A Thesis

Submitted to the Graduate Faculty of the
Louisiana State University and
Agricultural and Mechanical College
in partial fulfillment of the
requirements for the degree of
Master of Science in Civil Engineering

in

The Department of Civil and Environmental Engineering

by
Ananth Bukkapatnam Tirumala
Bachelor of Technology,
Sri Venkateswara University, India, 2005
December 2008

ACKNOWLEDGMENTS

I express my deep sense of appreciation to my advisor Dr. Radhey S. Sharma for his immense support and invaluable suggestion. With his knowledge and experience, he continuously guided me towards my goal of completing this work. I express gratitude for his patience, time, help and support. I am grateful to him for his selfless support and guidance bestowed during the course of my study. I am indebted to him for the encouragement he provided.

I thank Dr. Khalid Alshibli and Dr. Murad Abu Farsakh for being on my committee and for the knowledge they imparted towards my Master's degree. I also thank Dr. Guoping Zhang for his support. Special thanks to Kiran, Srikanth, Mahendra, Bashar, Zhongxin for supporting me throughout. I am also thankful to my lab mates Sukanta, Pratima and Devraj for their enormous help and for all the time we spent together. I thank Ignacio for his valuable comments on my thesis.

I am indebted to my parents for their help and support throughout my career. Special mention is needed to my Sister Vasantha, Brother Srikanth, Aunt Padmini Tamirisa and Uncle Sudhakar Tamirisa for their love and support. I was fortunate to have encouragement and support from all other family members and friends. I would like to thank everyone at LSU who played their role to make my program pleasurable and successful. Finally, I would like to thank God Almighty for giving me this precious life so that I could make it meaningful and colorful.

TABLE OF CONTENTS

LIST OF TABLES

LIST OF FIGURES

NOTATIONS

The following symbols are the important notations and acronyms used in this research study.

G_{max} – Small strain stiffness

V_s – Shear wave velocity

ρ – Soil mass density

ρ_d – Soil dry mass density

γ – Soil unit weight

γ_d – Soil dry unit weight

σ' – Effective stress

$u_a - u_w$ – Matric Suction

u_a – Pore air pressure

u_w – Pore water pressure

S_r - Degree of saturation

e – Void ratio

L_s – Length of the specimen (Effective length between bender elements)

t_s – Time taken by the shear wave to travel one length L_s of the specimen.

SWCC – Soil water characteristic curve

BE – Bender element

UU – Unconsolidated undrained

ABSTRACT

Soil stiffness is a strain dependent non-linear parameter. Stiffness is the measure of soil deformation under a particular working load. It can used for predicting ground deformation in engineering earthworks such as highway embankments and foundations. Non-linear analyses for ground behavior have been widely used for developing models to predict the small –strain characteristics of the soil (Atkinson, 2000). This thesis provides a new insight into the behavior of soil stiffness. We used the wave propagation technique to determine the stiffness and term it as the small strain shear modulus (G_{max}) of the soil. The objective of the thesis was to predict the influence of wetting/drying cycles on unsaturated soil shear stiffness.

Low-plasticity Silty Clay (CL) was tested to determine the variation of soil stiffness along its wetting/drying path using a one dimensional soil water characteristic curve apparatus and an unsaturated triaxial cell. The pore water pressure of the soil was zero as it was open to atmosphere. Soil samples that were compacted to the optimum moisture content using standard Proctor test were used in the experiments. Tests were conducted using the axis translation technique and it was observed that the stiffness of the soil increased with increase in soil matric suction. Significant hysteresis was found in the behavior of stiffness along the wetting path and its value was more than the value of the stiffness along the drying path at the same pressure. Soil samples compacted at 2, 4 , 6% dry of standard Proctor optimum were used and subjected to wetting to find the variation of stiffness with moisture content. Stiffness was found to decrease with increase in moisture content both along the dry and wet sides of optimum. Influence of consolidation on stiffness was investigated. Stiffness was found to increase with increase in consolidation pressure. Stiffness was found to increase with the undrained shear strength, tested using the unconsolidated undrained (UU) triaxial test. Statistical analysis was used to develop a statistical fit model of the results, within fixed limits of matric suction and the soil stiffness.

CHAPTER 1 INTRODUCTION

Geotechnical engineering is a branch of civil engineering field which is strongly rooted in relating engineering mechanics to solving problems related to strength, strain, and seepage of soils. Karl Terzaghi, "Father of Soil Mechanics", proposed the coveted "effective stress principle for saturated soils" which has been the cornerstone in formulating geotechnical principles, analyzing and evaluating field projects related to soils and using it in different zones of the world. Various researchers have worked on the effective stress principle proposing several nuances to it and one such proposal being the "stress state variable approach" useful in describing the behavior of unsaturated soils and practicing it in different areas around the globe. Jardine (1994) studied various case histories for piles, excavations etc. in different types of soils, analyzing the overall ground movement at typical working loads predicting that the ground strains typically range between 0.001-0.5%.

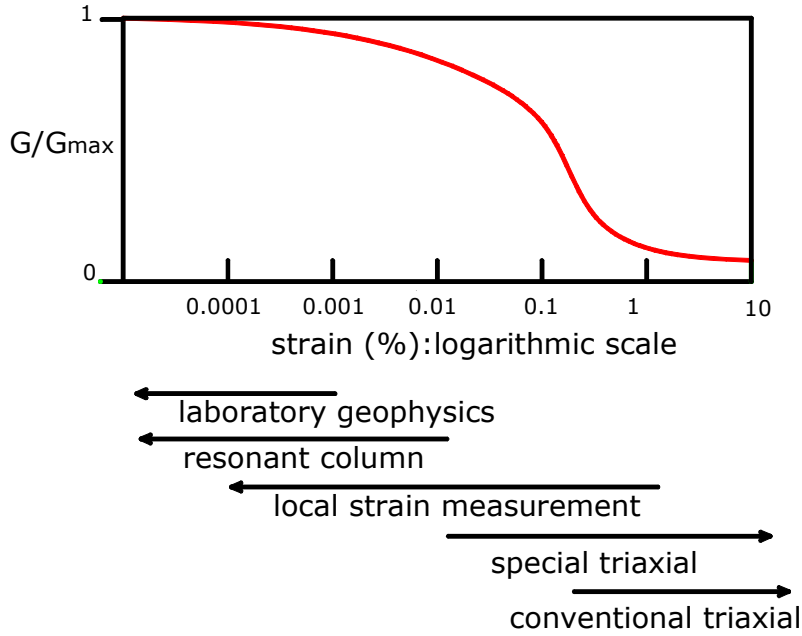

FIG 1.1: Least count for strains of different methods used to measure stiffness (Atkinson and Sallfors, 1991)

Arid and semi-arid regions comprise more than one-third of the earth's surface. Soils in

these regions are dry and desiccated near the ground surface. These conditions may extend to a considerable depth and in some cases the water table may be more than 30 meters below the ground surface. Even under humid climatic conditions the groundwater table can be well below the ground surface and the soils used in construction are unsaturated in nature. Compacted soils comprise a large part of the earth structures designed by engineers.

Problematic unsaturated soils such as residual soils, swelling clays, collapsible soils are difficult to be tested in the laboratories due to one common phenomenon called negative pore-water pressure which affects the mechanical behavior of these soils. The mechanical behavior of a soil is governed by it strength, strain and seepage. This thesis deals with the assessment of the characteristic stress strain behavior of soils for monotonic loading and to assess the behavior of small strain shear modulus of soils at very small strains during cycles of wetting and drying and along the compaction curve of the soil.

Furthermore, geotechnical engineers increasingly use elastic wave-based geophysical and non-destructive evaluation techniques to image and gather more information about the near subsurface. However, elastic wave speeds are directly dependant on the effective stresses and capillary forces that control the stiffness of soils. For all these reasons, understanding the low and high strain behavior of unsaturated soils is essential in the advancement of research and practice of geotechnical engineering today. Deformation of the structures under loads depends on the soil on which the structure rests which requires the behavior of the particles at very small strains. Stiffness of the soil is a function of the small strain shear modulus (G_{max}) of the soil.

1.1 Research Background

Engineering structures often encounter very small strains due to static loads. Shear strain was distinguished as 3 patterns by Atkinson and Sallfors (1991) in Figure 1.1. At very small strains of 0.001%, the shear modulus is nearly constant with strain. For strains larger than the yield strain

and less than 1%, the shear modulus is a non-linear function of strain and at strains greater than 1%; shear modulus is very small as the soil tends to fail. Very small strains are caused due to soils response to both static and dynamic loads. The shear modulus at very small strain (G_0) is also referred to as the maximum shear modulus (G_{max}). In this research, G_{max} is used to describe the stiffness characteristics of the soil.

Small strain shear modulus (G_{max}) for saturated soils has gained a lot of research importance during the past decade relating it to the stress state and the current volumetric state of the soil (Jovicic, 1997) and biaxial confinement proving G_{max} is a directional property. All these tests were performed on saturated soils leaving the research aspects of unsaturated soil conditions yet to be performed. Cabarkapa et al (1999) developed a constitutive model to relate G_{max} and the matric suction for unsaturated soils. In this research, we try to analyze the dependency of G_{max} on the wetting and drying cycles of a soil and along the compaction curve, including the wet and dry of optimum. Experimental data resulting from a series of tests proposed in this study will prove extremely valuable for all of the following

- Stiffness of unsaturated soils along the wetting/drying cycles.
- Nature of hydraulic hysteresis.

1.2 Objectives of the Research

The following are the main objectives of this thesis:

1. Study the influence of matric suction on the small-strain shear modulus along the wetting/drying paths of the soil water characteristic curve.
2. Evaluate the hysteresis of the soil water characteristics curve.
3. Study the variation of small-strain shear modulus along the compaction curve.
4. Compare the results of this investigation and related the small strain shear modulus to study its variation against consolidation pressure and the undrained shear strength of the

soil.

1.3 Thesis Outline

The thesis consists of six chapters including this introduction.

Chapter 2 presents the motivation of this thesis and literature review about unsaturated soils and their mechanical behavior. Details regarding the soil water characteristic curve and the small strain shear modulus are presented with the pros and cons of their determination.

Chapter 3 gives the details of the apparatus used for the research along with the modifications and specifications. Installing the testing system together and procedures for testing are included in detail with relevant figures and explanations. The type of soil used and its engineering properties are presented at the beginning of this Chapter discussion.

Chapter 4 includes the results gathered explaining the conditions at which they were collected and a general procedure on how they were collected. The effect of matric suction (u_a-u_w) on the small strain shear modulus of soils (G_{max}) is shown with all the calculations explained. The change in stiffness (i.e., small strain shear modulus of soils, G_{max}) along the compaction curve is also presented. Stiffness measurements are done against the variation of consolidation pressure and also its variation with undrained shear strength. All the results are thoroughly analyzed and discussed.

Chapter 5 discusses the statistical regression analyses for the results obtained and the best possible fit for the data obtained is presented in this chapter.

Chapter 6 summarizes the conclusions of this investigation and presents recommendations for future research.

CHAPTER 2 LITERATURE REVIEW

2.1 Unsaturated Soils

Early insight into geotechnical engineering took place in the North Eastern regions of United States and in Western Europe due to heavy rainfall in these regions. Studies on different soils were conducted considering the saturated condition of the soils at these regions. Even under wet climatic conditions the groundwater table can be well below the ground surface and the soils used in construction are unsaturated. Compacted soils comprise a large part of the earth structures designed by engineers such as bridges, tunnels, submerged pipelines etc.

Saturated soils can be found at places where the precipitation is high or below ground water table, with air and water phases evaluating their behavior. Processes like evaporation and evapo-transpiration make the ground surface dry leaving the soil unsaturated. In unsaturated soils, both air and water occupy the pore space. Unsaturated soils are three-phase materials, comprising soil solids, water, and air. In principle, a phase is identifiable in a medium when it has matter, distinctive properties, and a clear limit. In soils, no phase is readily identifiable because of the difficulty in visual identification and the non-homogeneous nature of the soil. To explain the behavior of unsaturated soils, Fredlund and Rahardjo (1993) recognize the air-water interface, the so-called contractile skin, as an additional phase that acts as a stretched membrane between the air and water phases. Surface tension is the most important parameter in analyzing the contractile skin in unsaturated soils. Most soils used as construction material are in compacted condition and may be unsaturated for long periods of time that will be subjected to wetting-drying cycles due to the change in moisture content of the soils at different climatic conditions.

The behavior of unsaturated soils is of importance in a widerange of geotechnical and environmental engineering projects. Examples can be found in earth dams, transportation

projects (e.g., highway and railway embankments), and also in environmental projects (e.g., cut-off walls and clay liners at landfill sites). Effective stress principle, developed by Karl Terzaghi, is the key concept that has led to the rapid transfer of geotechnology around the world. The effective stress principle was mainly developed for saturated soils which was later extended to unsaturated soils. Phenomena like capillarity, suction, swelling and shrinking are of utmost importance in understanding the behavior of unsaturated soils.

In this Chapter, concepts and the methodology of the small strain parameters in unsaturated soils are reviewed. The use of piezo-ceramic bender elements and their functionalities and the propagation of elastic waves in soils are discussed in the subsequent Chapters in detail. Results from previous published literature were analyzed with their relevance to the ongoing research and discussed in detail. This chapter mainly discusses the current common methods used to determine the stiffness of soils in the laboratory.

2.2. Characteristics of Unsaturated Soils

Saturated soil are divided into three phases constituting solids, air and water phases. The constitutive behavior of a soil can be described in terms of the state of stress in soil. The state variables describe the state of a system that requires information for the complete characterization of the system. The volume change behavior and the shear strength characteristics of a saturated soil are governed by the effective stress and are commonly expressed in the form of Equation 2.1.

$$\sigma' = \sigma - u_w \tag{2.1}$$

σ' = Effective normal stress; σ = Total normal stress; u_w = Pore-water pressure.

The effective stress principle is a stress state variable that can be used to describe the behavior of saturated soil and is applicable to all soils because it is independent of the soil

properties. The validity of the effective stress as a stress state variable for saturated soils has been well accepted and experimentally verified (Bishop and Eldin, 1950; Skempton, 1960).

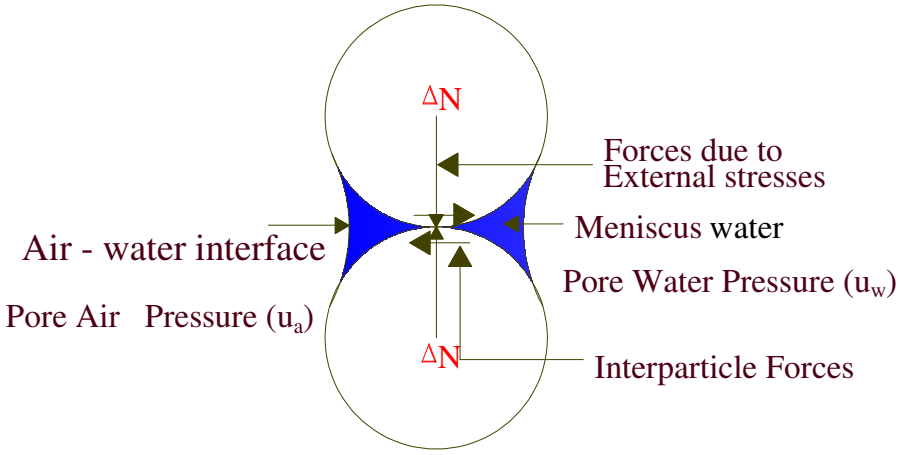

FIG 2.1: Typical contact parameters of unsaturated particulates (Sharma, 1998)

The use of a single variable for the effective stress equation is not valid for unsaturated soil because the stress induced by suction in meniscus water acts differently on the soil particle compared to the external normal stress acting on the particle. This is illustrated in Figure 2.1 where the contact of two idealized spherical particles is considered. The application of external stresses develop normal and shear inter-particle forces at the contact but the introduction of matric suction causes additional inter-particle normal forces (ΔN) due to the meniscus water at the contact. These additional normal or inter-particle forces result in slippage of particles at the contact causing an increase in shear strength, increase in elastic compression causing an increase in the effective stress. Plastic strains develop due to the additional normal forces to prevent slippage of particles causing a decrease in effective stress for unsaturated soils.

The use of a single valued effective stress for unsaturated soils has encountered many difficulties because unsaturated soils are viewed as a three phase system (Lambe and Whitman, 1969) and the incorporating the soil properties in the description of the stress state leads to

difficulties such as predicting the volume change behavior of these soils.

Stress variables used for the description of a stress state should be independent of soil properties (Fung, 1977) and it has led numerous researchers to the realization that two independent stress state variables should be used for unsaturated soils and the effective stress equation has been separated into two independent stress variables i.e. $(\sigma - u_a)$ and $(u_a - u_w)$ to describe the mechanical behavior of unsaturated soils. Many researchers have developed different equations (Equation 2.2 to Equation 2.7) to determine the effective stress of unsaturated soils. The following are the examples:

$$\sigma' = \sigma - \beta' u_w \qquad \text{(Croney et al., 1958)} \qquad (2.2)$$

$$\sigma' = (\sigma - u_a) + \chi(u_a - u_w) \qquad \text{(Bishop, 1959)} \qquad (2.3)$$

$$\sigma' = \sigma + \psi\, p'' \qquad \text{(Aitcheson, 1961)} \qquad (2.4)$$

$$\sigma' = \sigma + \beta p'' \qquad \text{(Jennings, 1961)} \qquad (2.5)$$

$$\sigma' = (\sigma - u_a) + \chi_m (h_m - u_a) + \chi_s (h_s + u_a) \qquad \text{(Richards, 1966)} \qquad (2.6)$$

$$\sigma' = \sigma + \chi_m p_m'' + \chi_s\, p_s'' \qquad \text{(Aitcheson, 1965, 1973)} \qquad (2.7)$$

Where,

σ' = Effective normal stress.

σ = Total normal stress.

u_a = Pore air pressure.

u_w = Pore water pressure.

β' = The holding or bonding factor which is a measure of the number of bonds under tension, effective in contributing to the shear strength of the soil.

χ = A parameter related to the degree of saturation of the soil.

ψ = A parameter with values ranging from zero to one.

p'' = Pore water deficiency.

β = A statistical factor of the same type as the contact area. This factor should be measured experimentally.

χ_m = Effective stress parameter for matric suction.

h_m = Matric suction.

χ_s = Effective stress parameter for solute suction.

h_s = Solute suction.

p_s'' = Solute suction.

p_m'' = Matric suction.

These researchers have concluded that any two of three possible normal stress variables can be used to describe the stress state of an unsaturated soil, these are: 1) (σ-u_a) and (u_a-u_w). 2) (σ-u_w) and (u_a-u_w) 3) (σ-u_a) and (σ-u_w). Fredlund and Rahardjo (1993) claimed the use of mean net stress (σ-u_a) and matric suction (u_a-u_w) to describe the mechanical properties of unsaturated soils. The stress state variables can then be used to formulate constitutive equations to describe the shear strength behavior and the volume change behavior of unsaturated soils. These components affect the deformation characteristics of the soil and hence the stiffness of the soil.

2.3 Shear Strength and Volume Change Characteristics of Unsaturated Soils

2.3.1 Shear Strength

Shear strength of unsaturated soils can be expressed in terms of two stress state variable, net stress and matric suction ((σ-u_a) and (u_a-u_w) respectively) as proposed by Fredlund et al (1978) and is given by Equation 2.8. Escario and Saez (1986) showed that the shear strength of unsaturated soil increases non-linearly with suction. Gan et al (1988) showed that the friction

angle with respect to suction φ^b is equal to φ' for suction less than the air entry value and thereafter, decreases for an increase in the value of suction. Also, Escario and Juca (1989) showed that the shear strength began to decrease for very high values of suction.

$$\tau = c' + (\sigma - u_a) \tan \phi' + (u_a - u_w) \tan \phi^b \quad (2.8)$$

Where, φ' – friction angle of the soil and φ^b is the friction angle for suction less than the air entry value.

The most frequent tests used to measure the shear strength of a soil in the laboratory are direct shear test and triaxial test. The unsaturated triaxial test is performed on a cylindrical soil specimen enclosed in a rubber membrane, placed in the triaxial cells. Compared to the regular triaxial end platens, the platens used for testing unsaturated soil have a high air entry ceramic stone and a low air entry filter embedded in the top and bottom platens so as to apply the necessary pore air pressure and the pore water pressure to the soil sample so as to reach a specific value of matric suction. In this research study one such equipment is used to determine the hysteretic nature of the soil and also to analyze the stiffness of the soil at particular matric suction. The details of the equipment are discussed in the subsequent chapters. Various triaxial tests are used for unsaturated soils based upon the drainage conditions during the first and second stages of the triaxial test. The different triaxial tests performed on unsaturated soils are consolidated drained (CD) test, constant water content (CW) test, and consolidated undrained (CU) test with pore pressure measurements, undrained test and unconfined compression test. In the CD test, CW test and CU test, the soil specimen has a net confining pressure of $(\sigma_3 - u_a)$ and a matric suction $(u_a - u_w)$ at the end of the consolidation process and during the shearing phase, the soil specimen is compressed in the axial direction, till the soil fails in shear. The pore water pressure is drained in CD test, pore air pressure is drained in CW test and both the parameters

remain undrained in CU test during the shearing phase of the soil. In an undrained test, the pore water pressure parameters are not allowed to drain during the application of confining pressure and the deviator stress.

The shear strength data obtained from triaxial tests can be analyzed using the stress state variables at failure or using the total stresses at failure when pore pressures are not known. This concept is similar to the effective stress approach and the total stress approach used in saturated soil mechanics. In a drained test, the pore pressure is controlled at a desired value during shear. Any excess pore pressures caused by the applied load are dissipated by allowing the pore fluids to flow in or out of the soil specimen.

The pore pressure at failure can be used to analyze the shear strength data. In an undrained test, the excess pore pressure due to the applied load can build up because pore fluid flow is prevented during shear. If the changing pore pressures during shear are measured, the pore pressures at failure are known, and the stress state variables can be computed. However, if pore pressure measurements are not made during undrained shear, the stress state variables are unknown. In this case, the shear strength can only be related to the total stress at failure. Fredlund et al (1995) suggested that the shear strength could be predicted from the soil water characteristic curve relating matric suction (u_a-u_w) and degree of saturation (S_r).

2.3.2 Volume Change Behavior

Collapse on wetting at higher net stresses and wetting induced swelling at lower net stresses is the most common feature of unsaturated soil volume as proven by Matyas and Radhakrishna (1968). Fredlund and Morgenstern (1977) suggested state surfaces for void ratio (e) and water content (w) representing a planar surface. Lloret and Alonso (1980) suggested state surfaces for void ratio (e) and degree of saturation (S_r). These state surfaces could represent both swelling and collapse of soils during the wetting phenomenon. However, the behavior of soils during

drying or unloading does not invariably affect the behavior of unsaturated soils. Matyas and Radhakrishna (1968) also reported that the state surfaces induced by wetting are limited to the virgin-loading conditions of the soil and the drying paths follow the swelling surfaces which lie under the virgin loading line.

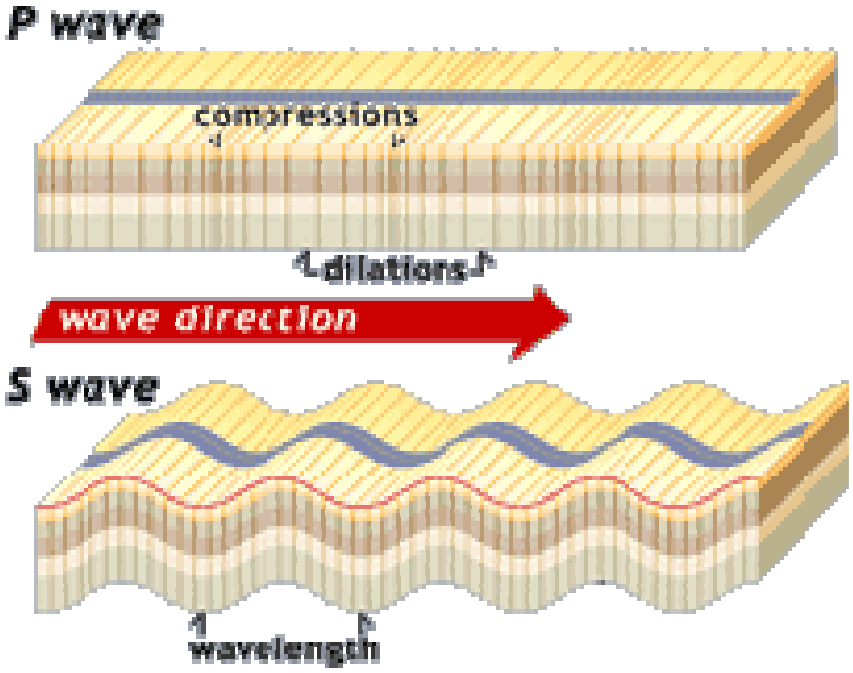

FIG 2.2: Typical elastic wave propagation in a medium (google.com/images/p and s waves)

2.3.3 Stiffness

Soil stiffness is a measure of the deformation of a soil at an applied load over a period of time. Soil stiffness was traditionally determined while performing triaxial tests and resonant column tests using high precision strain gauges capable of a least count of 0.001%. These tests were tedious and required a lot of skill to be performed and were difficult to perform at strains smaller than 0.001%. More recently, stiffness gauges have been used to determine stiffness of soils in-situ. To measure the small strain stiffness (G_{max}) of soil at strains as low as 0.0001% in the laboratory, the use of piezo-ceramic elements have gained importance and the study of wave

propagation in soils brings clarity to the measurement of stiffness of soils with the pros and cons discussed in the literature review.

2.4 Wave Propagation in Soils

Elastic waves are small mechanical disturbances causing no permanent effects to the medium or altering already occurring phenomenon (Santamarina et al. 2001). Elastic waves are classified as P or Compression waves propagating along the longitudinal direction of motion in the medium and S or Shear waves propagating perpendicular to the direction of motion in the medium shown in Figure 2.2. Usually, the P-waves propagate faster than an S-wave due to their smaller wave lengths and higher frequencies. In this study, we analyze the shear stiffness of the soil and hence use S-waves in our study. Both the types of waves are generated at the same time and hence, certain standard specific dimensions of the medium of measurement are necessary to nullify the effect of the P-waves.

$$V_s = \sqrt{\frac{G_{\max}}{\rho}} \tag{2.9}$$

In general, waves produce very small disturbances in the soil and hence very small changes in their strain levels. These small strains fall in the linear portion of the stress – strain curve with reference to Hooke's law and hence, the modulus at this point of the curve is considered maximum. Hence, in this study we measure, the maximum shear modulus (G_{max}) of the soil relating it to the shear wave velocity (V_s). Shear wave velocity is a function of the small strain shear modulus (G_{max}) and the particle density (ρ). Equation 2.9 shows the relationship between shear modulus and the shear wave velocity.

The shear wave velocity depends on the stress state, particle orientation and the degree of saturation of the soil. Shear wave velocity increases with increase in stresses and denser particle orientation and decreases with degree of saturation (S_r) as presented by Fratta et al, 2001.

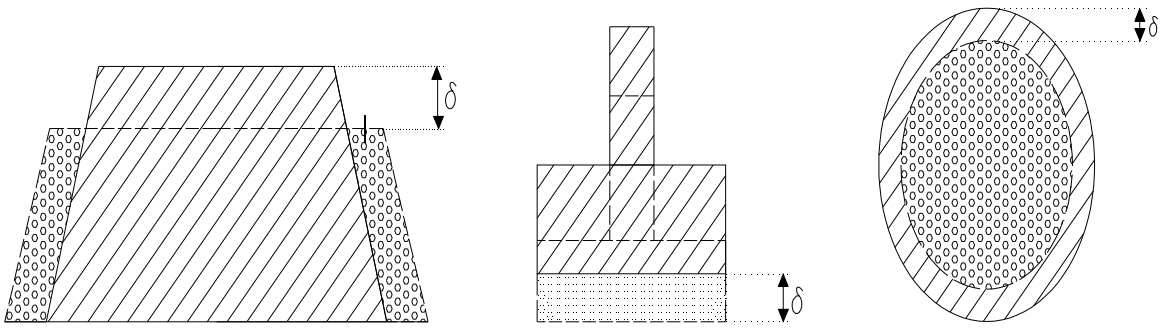

(a) (b) (c)

FIG 2.3: Examples of geotechnical structures requiring soil stiffness in their design

2.5 Stiffness of Soils

Understanding the low and high strain behavior of unsaturated soils is essential in the advancement of research and practice of geotechnical engineering today to carefully evaluate the deformation of the soil under subjected loads which in other terms is the stiffness of the soils. The Figure 2.3 shows some examples of geotechnical structures which require the measurement of soil stiffness at small strains in their design assuming greater importance in the study of soil mechanics and its applications to geotechnical design (Matthews et al. 2000; Stokoe and Santamarina 2000). The back calculations of horizontal and vertical movement performed from the static field measurements of strain are compared to dynamic laboratory measurements in the small strain zone where G_{max} is evaluated. Settlements of embankments, foundation, tunnels, and movements along the front and back of retaining walls can be calculated using G_{max} values. Furthermore, small-strain behavior of soils is paramount in predicting performance of earth structures during construction and subsequent working stages (Brand, 1981; Macari and Hoyos, 2000; Vinale et al., 2001).

The study of the behavior of particulate media at very small strain is important to evaluate deformation of soils and thus of structures at working loads. The value of the shear

modulus at very small strains (G_{max}) is considered a fundamental soil property to determine its stiffness. This unit reviews concepts related to the small strain parameters in soils and the current methods used to measure them in the laboratory. Consequently, details of elastic wave propagation are introduced and the use of bender elements to generate and monitor elastic waves to measure the stiffness was developed.

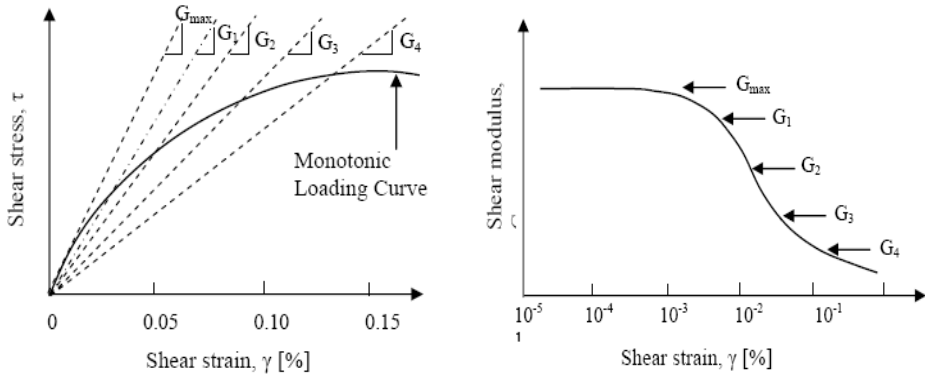

FIG 2.4: Non-linear behavior of stiffness (Atkinson, 2000)

Recently it has been shown that the stiffness of soil is highly non-linear at very small strains and its determination is highly critical in evaluating the strength and deformation of the soil (Atkinson, 2000). Results from previous research on the use of bender elements for saturated soils to measure the velocity of propagation of shear waves are included. The typical variation of shear or bulk stiffness with strain for most soils is given in Figure 2.4. The curve depicts non-linear soil stiffness from very small strains to pre-failure conditions. It is known that the strain-dependent curve depends mainly on soil plasticity in fine soils (Vucetic and Dobry 1991) and is affected by the mean effective stress in coarse soils (Ishibashi and Zhang 1993). Furthermore, it is believed that most soils behave elastically at very small strains (i.e., strain smaller than 0.001%) giving rise to a constant stiffness. The strain induced by the propagation of seismic waves is within this range and hence provides a measure of the upper bound for stiffness (G_{max}). The upper bound stiffness is clearly a fundamental parameter in defining this curve and

hence the use of seismic measurements of stiffness is becoming more relevant.

Also, the calculation of stiffness for unsaturated soils cannot be compared to the saturated soils as the capillary forces and the inter-particle contact forces play a significant role in its determination which is not the case with saturated soils. The capillary force is a function of the matric suction of the soil which is the difference in the pore air pressure and the pore water pressure. These parameters are generally excluded in many engineering activities but when it comes to evaluation of strength, stiffness and volume change behavior of the soil, matric suction plays a significant role in evaluation and estimation of these parameters. In this study, a new equipment to evaluate the wetting-drying characteristics of unsaturated soil and the use of the same to determine the stiffness of the soil is to be presented. Difficulties in incorporating the bender elements within the chamber lead to preparation of more number of specimens to evaluate the soil stiffness for each particular increment in the air pressure. The water contents of each specimen were measured to accurately determine the degree of saturation at the time of measurement.

2.6 Factors Affecting Stiffness of Unsaturated soils

2.6.1 Stress State

Hardin and Richart (1963) conducted tests on sand and showed that shear wave velocity depended on the void ratio and confining pressure. They showed a linear relationship between these parameters. They also suggested a linear relationship for clays which was later modified to bring in dimensional equity in Equation 2.10 suggested by Hardin and Black (1968).

$$G_0 = Sf(e)OCR^k p_a^{(1-n)} (p - u_w)^n \qquad (2.10)$$

Where, S is a dimensionless modulus of soil structure, OCR is the over-consolidation ratio dependant on the plasticity index with k as the corresponding power coefficient, p_a is the air

pressure and ($p-u_w$) is the effective stress and n is a power coefficient usually equal to 0.5 for a variety of materials tested.

Stokoe et al (1985) suggested that G_0 doesn't depend on the effective stress which is normal to the shearing plane. Their conclusions predict an anisotropic stress state leading G_0 as an anisotropic parameter. Their findings were limited to the experiments conducted on sands, as for clays, a small increase in the effective stress causes invariable volume changes which later affect G_0 (Jovicic et al, 1996). Stiffness (G_0) of soil has been considered to be highly non-linear as suggested by all the above researchers. Based on these findings, Hardin and Blandford (1989) modified the empirical relation as shown in Equation 2.11 and Equation 2.12.

$$G_{0(ij)} = \frac{OCR^k}{f(e)} \frac{S_{ij}}{2(1+\nu)} p_a^{(1-n)} (\sigma'_i \, \sigma'_j)^{n/2} \tag{2.11}$$

Where, $f(e) = 0.3 + 0.7e^2$ (2.12)

Also, $G_{0(ij)}$ is the shear modulus in the plane of principal stresses σ'_i, σ'_j, while $2(1+\nu)$ shows the effect of poisson's ratio, S_{ij} is a dimensionless parameter defining the soil structure and OCR is now a function of ($p-u_w$).

For isotropic soil, shear modulus is a vector since it is correlated to the product of biaxial compressive effective stresses (σ'_i and σ'_j). It is not clear how $G_{0(ij)}$ represents the stress state because soil cannot be solely in a condition of biaxial compression.

2.6.2 Soil Structure

Structural anisotropy develops due to different sizes and orientation of particles in the soil. This anisotropy causes variation in the soil properties and also is different from stress induced anisotropy. In order to separate these two out, the soil is always tested in an isotropic stress state. Structural or inherent anisotropy is a result of geological formation and also can be man- made with examples of fills and embankments. This man-made anisotropy is strain induced. Sands are

less affected by strain deformation but for clays, the change in the orientation of the particles causes large strains and hence the inherent anisotropy will be large if not completely transformed by straining.

Soil structural anisotropy can be determined by dynamic methods where the soil specimen used to determine stiffness is placed and tested with principal axis coincident to its axis. This means that the principal axes of the fabric is known and to assume some kind of anisotropy since, the waves propagating through the soils may sometimes be neither shear nor compressive making their interpretation difficult.

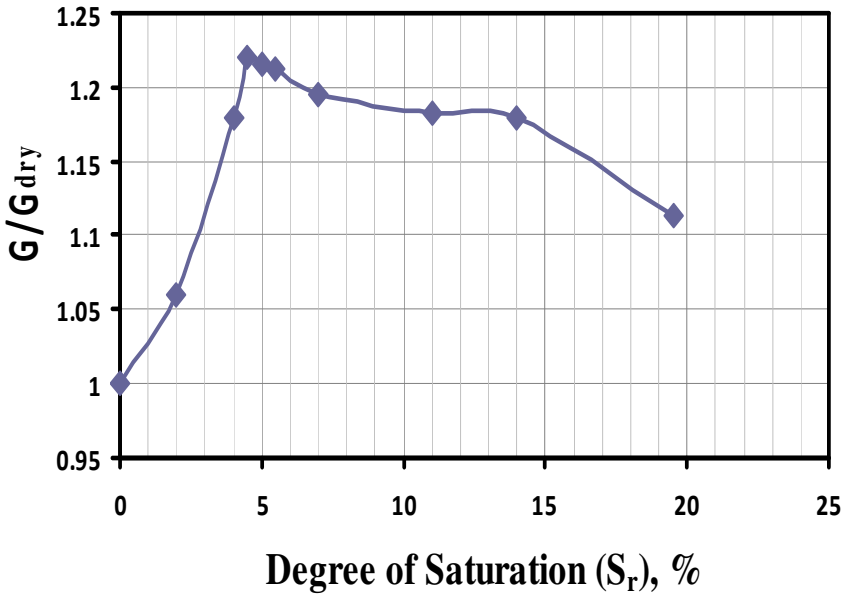

FIG 2.5: Shear stiffness of R1 sand vs. degree of saturation (S_r) (Qian et al., 1993)

2.6.3 Matric Suction

The soil conditions in arid and semi-arid climatic conditions are generally unsaturated in its natural or compacted state. The influence of the contractile skin on the mechanical behavior of unsaturated soils has been studied by several researchers (Fredlund et al, 1978). Several experiments and modeling have been conducted with limited exposure to the exact behavior of these soils. The influence of matric suction on the shear modulus is one phenomenon which

needs considerable attention. The water present in the contractile skin exerts a negative pore pressure on the particles contributing to the effective stress of the soil thereby increasing the shear strength. Also the changes in the water content due to wetting, drying or due to rainfall infiltration can contribute to a change in the inter-particle forces or inter-granular stresses affecting the shear modulus of the soil.

Qian et al (1993) showed that the influence of degree of saturation on the small strain stiffness was largest for particles with small effective grain diameter and at low confining pressure. Qian et al (1993) also conducted resonant column tests on sands showing the change of G_0 with water content increases with the increase in percentage of fines in the soil. Figure 2.5 shows the variation of small stain stiffness normalized to the dry shear modulus versus degree of saturation and Figure 2.6 depicts the response of stiffness to increasing suction.

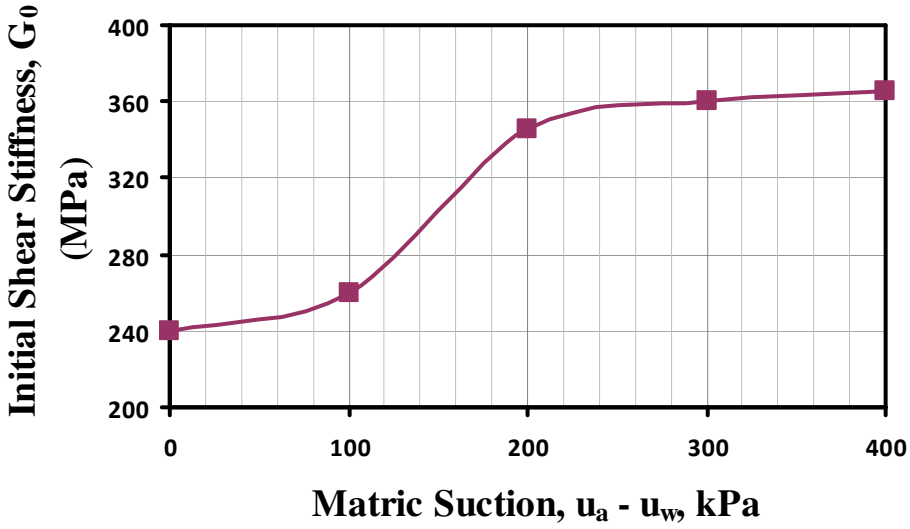

FIG 2.6: Response of shear stiffness to suction (Mancuso et al. 2002)

Mancuso et al. (2002) carried out an experiment using a controlled suction resonant column – torsional shear cell to analyze the small strain behavior of unsaturated compacted silty sand. Specifically, they analyzed the effects of suction and fabric on soil behavior. Shear stiffness measurements are taken during constant-suction tests. Their data indicated S-shaped

initial shear stiffness versus suction variation, which can be explained considering the progressive change from a bulk-water governed soil response to a menisci-water governed soil response. Most of the effects are detected for suctions ranging from 0 to about 200 kPa. For values higher than 200 kPa, G_0 tends toward a threshold that depends on the net stress level.

Marinho et al (1995) conducted tests on clay using bender elements and filter paper technique showing an initial increase in G_0 for specimens subjected to drying and leveling off with increasing suction.

Cabarkapa et al (1999) designed a modified triaxial cell to do tests of isotropic loading and unloading at controlled suction and have shown that similar to saturated soils, the shear modulus of unsaturated soils is high during unloading than during the loading cycle even though the mean net stress is the same. The details of the apparatus and the testing procedure are discussed in the following sections.

2.7 Soil Water Characteristic Curve

The plot between the gravimetric water content (w) or degree of saturation (S_r) or the volumetric water content (θ) versus the matric suction (u_a-u_w). The original plot for the soil water characteristic curve is between the volumetric water content (θ) versus the matric suction (u_a-u_w) but since the soil is considered incompressible, all the plots lead to the same information. The relationship between the degree of saturation (S_r), volumetric water content (θ) and gravimetric water content (w) is given in Equation 2.13**.**

$$\theta(1+e) = S_r e = wG_s \tag{2.13}$$

Where, G_s is the specific gravity and e is the void ratio.

2.7.1 Importance and Uses

The soil water characteristic curve is used to model the inflow and outflow of fluids in the soil assuming the net stresses are negligible (p-u_a=0) and the soil is incompressible. These

assumptions are inappropriate for geotechnical engineering considering the fact that the soil deformation is not considered.

The hysteretic nature of the soil water characteristic curve has been studied in great detail by various researchers and a typical plot of a soil water characteristic curve is shown in Figure 2.7. Saturated soils can have a significant value of suction at the boundary with no drop in the degree of saturation below unity (Bishop and Wesley, 1975) and the degree of saturation drops below unity when the applied suction is reduced to zero (Sivakumar, 1993).

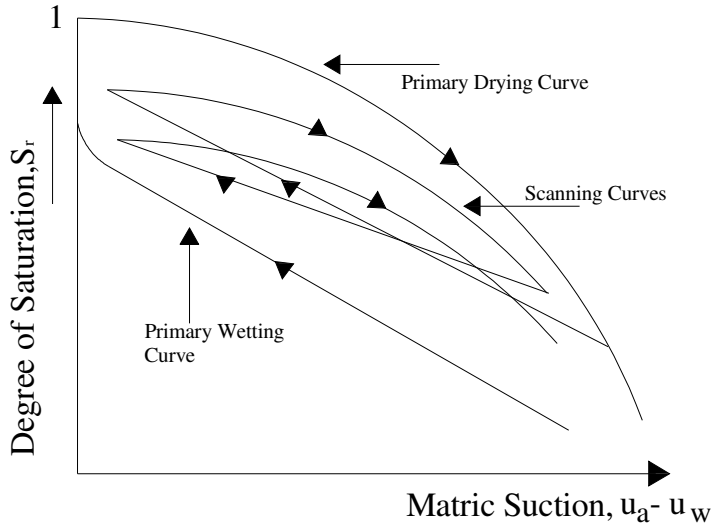

FIG 2.7: Hysteretic nature of the soil water characteristic curve

In Figure 2.7, the primary wetting and primary drying curve correspond to soils at fully saturated condition and the intermediate curves or the scanning curves correspond to soils subjected to previous wetting or drying. The contact angle during processes of wetting and drying and the entrapped air could be a reason for hydraulic hysteresis (Fredlund, 1993). This hysteretic nature of the curve is due to the differences in the volume of the meniscus water when subjected to cycles of wetting and drying. When the soil is subjected to drying, the meniscus shrinks and hence the matric suction will be high. When the soil is wetted, the meniscus tries to coalesce with other sections and hence the matric suction reduces.

At the same value of suction, the drying and the wetting curves give different values of degree of saturation; the mechanical behavior of the soil is affected by the hydraulic hysteresis of unsaturated soils and hence the shear strength and the volume change behavior of the soil is affected by this adverse behavior of the soil. Modeling of hydraulic hysteresis of soils have been effectively done by Sharma (1998) giving out constitutive relationships for soils. The soil water characteristic curve could also be generalized to determine soil properties such as shear strength and hydraulic conductivity and also the volume change characteristics of the soil.

2.8 Measurement of Small Strain Stiffness (G_{max}) in the Laboratory

The measurement of soil stiffness assumes importance in the study of soil mechanics and its applications to geotechnical design (Thomann and Hryciw, 1990; Viggiani and Atkinson, 1995a; Matthews et al., 2000; and Stokoe and Santamarina, 2000). Small-strain behavior of soils is important in predicting performance of earth structures. The behavior of soils at very small strains is important in assessing the deformation of the soils. The value of the shear modulus at very small strains (G_{max}) is considered a fundamental soil property.

Stiffness of soils can be measured both in-situ using experiments such as seismic wave analysis, cross- bore hole tests and laboratory experiments such as triaxial tests, oedometer tests and simple shear tests. Stiffness of the soil depends on the shear strength of the soil and hence can be related to the shear modulus (G_0) of the soil. In the recent past, small strain stiffness has been explored and hence convenient tests such as resonant column tests (Thomann and Hryciw, 1990) and piezo-ceramic bender element tests have been used in determining G_{max} (stiffness at very small strains) of the soil. Resonant column tests could be performed for a strain magnitude of 10^{-4}% and bender elements could be used for strains at 10^{-6}% (Thomann and Hryciw, 1990).

Estimation of stiffness is traditionally made in a triaxial apparatus using small deformation and displacement transducers. However these techniques are not precise enough and

cannot be used at very low strain levels. Dynamic methods for the measurement of soil stiffness at very small strains using resonant columns and, more recent, piezo-ceramic plates (bender elements) are used to provide better quality measurements of very low strain levels (Fiorovante and Capoferri, 2001). The evaluation of the shear wave velocity at small strains in the laboratory is typically performed under isotropic confinement using a resonant column device, but Thomann and Hryciw (1990) claim, "in situ soils are generally under a condition of no lateral strain during vertical loading, therefore the vertical and horizontal stresses may be quite different".

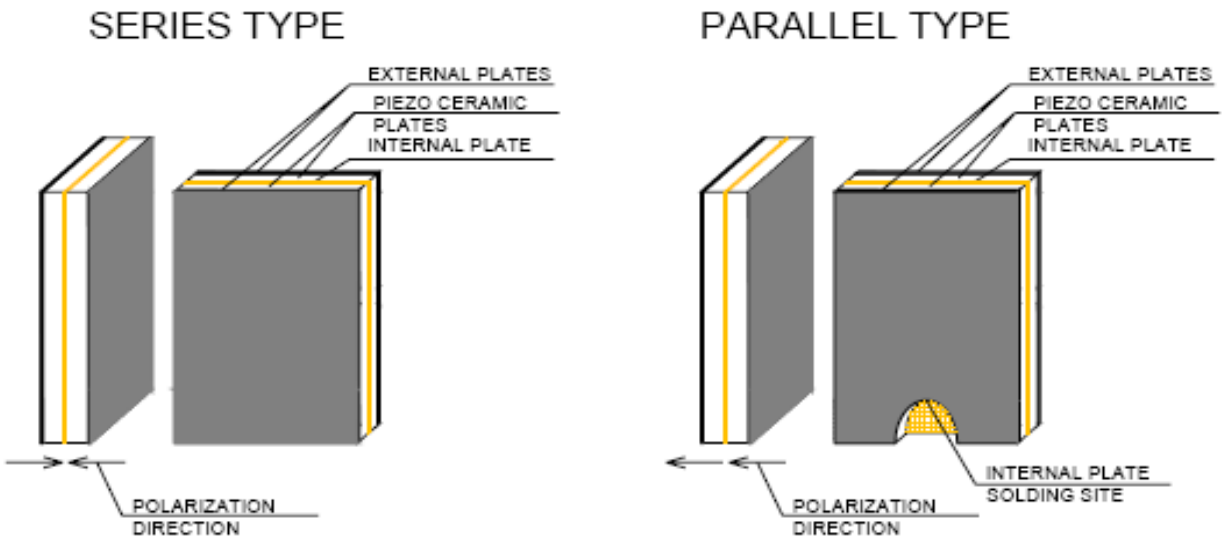

FIG 2.8: Bender elements mounted in series and parallel (Claudio et al, 2001)

Another commonly used technique uses bender elements to send and receive S-waves in soils. Piezo-ceramic elements distort or bend when subjected to a change in voltage (and generate a voltage when bent). Two such elements placed opposite one another provide a convenient measure of shear wave with one acting as the transmitter and other acting as the receiver. These elements consist of two transverse expander plates bonded together so that a voltage applied to the electrodes causes the plates to deform in different directions (one contracts in longitude while the other expands). This opposition causes the element to bend. Conversely,

mechanical bending of the element causes it to develop a voltage between the electrodes.

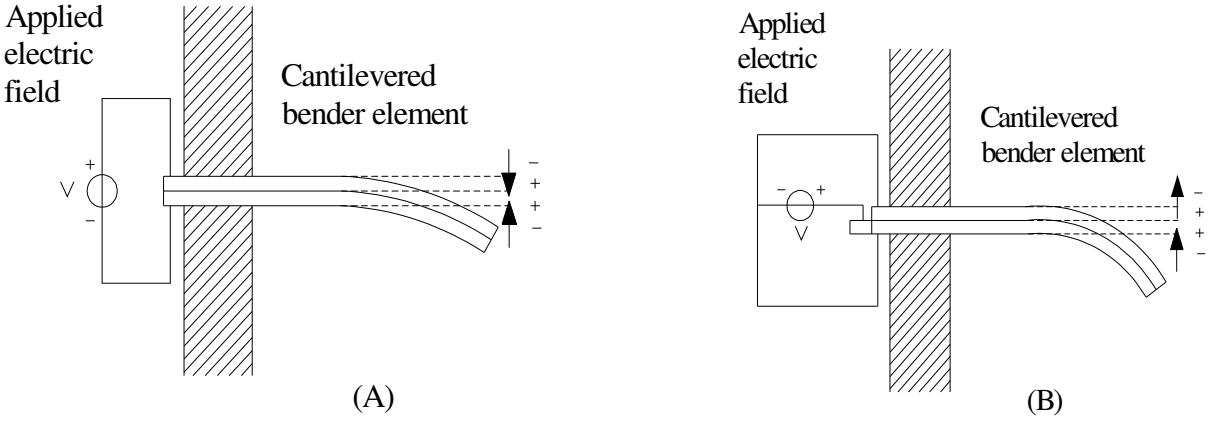

FIG 2.9: Cantilever (A) Series connected bender element and (B) Parallel connected bender element.

Bender elements may be assembled to operate in either series or parallel shown in Figure 2.8 and the deflection of these elements to voltage can be seen in Figure 2.9. The series elements develop twice the voltage as the parallel, but provide only half the displacement for the same applied voltage. Accordingly, a suitable setting should use a parallel bender element as the source and a series element as the receiver. In this research study, we adopt the use of two parallel bender elements to reduce energy losses and also for clear representation of the source signal unlike the combination of series and parallel elements as described before.

$$V_s = \frac{L_s}{t_s} \tag{2.14}$$

Where, V_s is the wave velocity, L_s is the distance between the tips of source and receiver bender elements, and t_s is the travel time. The dynamic elastic shear modulus G_{max} can be determined as,

$$G_{\max} = \rho . V_s^{\,2} \tag{2.15}$$

Where, ρ is the soil mass density and V_s is the shear wave velocity.

Equation 2.14 and Equation 2.15 form the basis of measurement for small strain stiffness

(G_{max}) of the soil using bender elements or any other piezo-ceramic elements. Mounted as cantilever beams, these bender elements are inserted within a small distance in a soil sample for the generation of elastic waves in the soil and for the reception of the elastic waves coming from the soil.

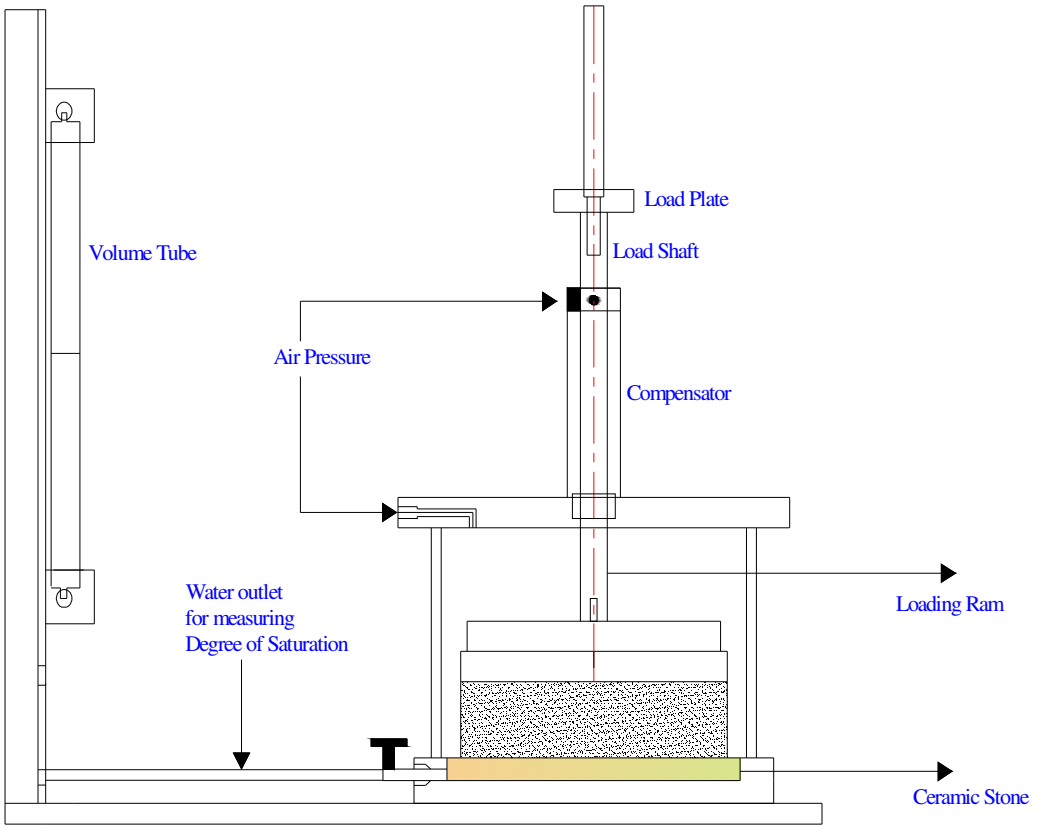

FIG 2.10: Instrument for measuring unsaturated stiffness along the drying path

The voltage in one element is varied which makes the bender element to vibrate. This vibration generates mechanical waves that propagate through the soil sample and are received by the opposite element, which converts the motion to an electrical signal. The input voltage (generated using a function generator) and the received signal are monitored using a digital oscilloscope, allowing the travel time to be determined.

The measurement of stiffness in unsaturated soils is also done using the same procedure but under a controlled suction environment using a special kind of equipment shown in Figure

2.10. This equipment is designed for evaluating the drying response of the soil specimen. The specimen is dried to a certain suction value and to a time until equilibrium is achieved. The specimen is then removed and tested for stiffness measurement. Though the suction is lost, the stiffness measurement is immediately taken after removing the specimen and a new specimen is prepared and dried to the same amount of time before application of a new pressure increment meaning that the rate of drying the soil is maintained.

Although measurements of small-strain shear wave velocities on soils using piezoelectric bender elements for determination of soil stiffness is feasible, the convenience of bender element tests is limited by subjectivity associated with identifying wave travel time and uncertainties surrounding the validity of some interpretation methods. Scholars (Arulnathan et al. 1998) performed studies aiming to improve understanding of the results from dynamic testing of soils using bender elements. Additional doubts exist regarding the influence of transducer support conditions on the characteristics of transmitted waves and the importance of reflected components on received waveforms (Dyvik and Madshus 1985; Viggiani and Atkinson 1995a, 1995b). The received signals can be distorted by near field effects, cross-talking, multiple reflections, etc.

Different methods to determine the travel times of elastic waves from piezo-ceramic bender elements for measuring the shear wave velocity of laboratory soil specimens have been proposed which are classified into two categories: time domain techniques and frequency domain techniques (Dyvik and Madshus 1985; Kawaguchi 2003). Currently there is no agreement regarding which method most closely estimates the true small strain stiffness of a soil. In this research study, we use the difference in the peak – peak time interval to determine the arrival time considering it to be precise and straight-forward in evaluating the small strain stiffness (G_{max}) of the soil.

2.9 Research Objectives

In this research study, the mechanical behavior of unsaturated soils are studied in detail with main emphasis on determining the small strain stiffness (G_{max}) along the wetting and drying paths of the soil using a variety of testing techniques as highlighted under

- The drying curve of the soil determined using a special device to determine the drying soil water characteristic curve.
- Measurement of stiffness of the soil using piezo-ceramic bender elements.
- Determination of the wetting and drying curve of the soil using a triaxial apparatus and also the stiffness of the soil along the wetting and drying curve.
- This test is aimed at suggesting a hysteresis in the behavior of stiffness when the soil is subjected to wetting and drying cycles.

The tests performed and their methodologies are clearly explained in chapter 3 and chapter 4 of this research study with all the drawings and details of the test given accordingly.

CHAPTER 3 MATERIAL PROPERTIES AND EXPERIMENTAL SETUP

3.1 Material Properties

3.1.1 Introduction

The soil used for testing and analysis is deep brown low plasticity clay (CL). The index properties of the soil are summarized in Table 3.1 and with the corresponding explanations in the sections to follow.

TABLE 3.1: Properties of low plasticity clay (CL)

Property	Value
Specific Gravity	**2.71**
Liquid Limit	**30**
Plasticity Index	**14**
Silt Content	**72%**
Clay Content	**22%**
Standard Proctor Maximum Dry Density	**17.36 kN/m^3**
Standard Proctor Optimum Moisture Content	**16.2%**

3.1.2 Specific Gravity

Specific gravity is a dimensionless quantity defined as the ratio of mass of the dry soil to the mass of equal water displaced. The test was conducted according to ASTM D854 using a pycnometer and was found to be 2.71.

3.1.3 Particle Size Distribution

Sieve analysis and the hydrometer tests were performed according to ASTM D422 and ASTM D2487-06 and respectively. Sieve analysis is used for particle sizes greater than 0.075mm (Sand

and Gravel) and the hydrometer analysis is used for particles smaller than 0.075mm (Silt and Clay). The particle size distribution is shown in Figure 3.1 (a). According to the unified soil classification system and the Casagrande's Plasticity chart, the soil can be classified as Low Plasticity Silty Clay (CL). The coefficient of uniformity (C_u) was calculated to be 50.91 and the coefficient of curvature (C_c) was 3.18. The percentage of silt and clay in the soil was found to 72% and 22% respectively. The soil was sieved in the sieve shaker before performing the actual test and the lumps of soil above the 4.75mm were broken into smaller divisions to facilitate sieving.

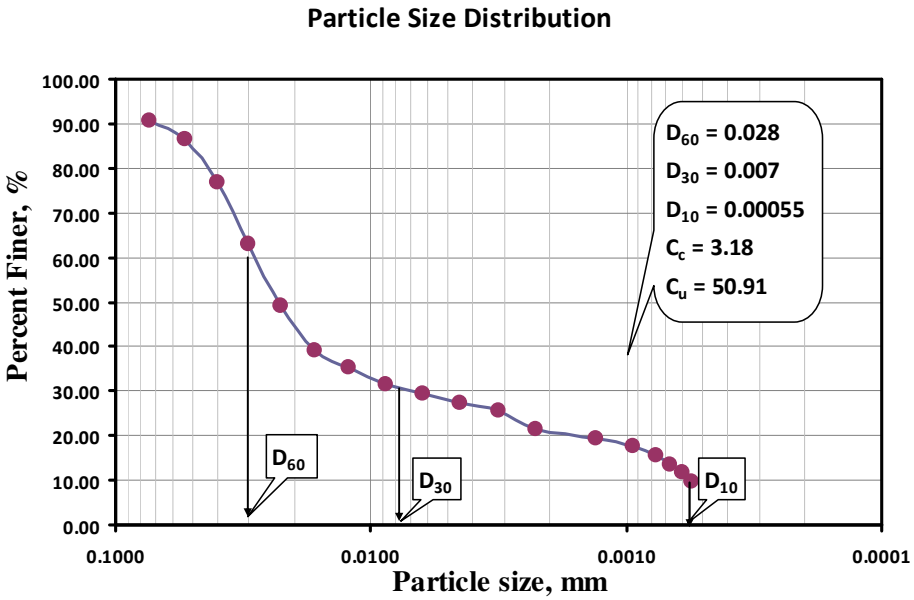

FIG 3.1(a): Particle size distribution of the soil

3.1.4 Compaction Test

Standard proctor tests were performed according to ASTM D698. The specimens used for determining the SWCC are trimmed out extracts of the compaction test. Soil after compaction is crushed and hence, new samples are prepared for every test performed. The compaction curve is shown in Figure 3.1(b) and the maximum dry density (γ_d) of the soil was found to be 1.736g/cc (17.36kN/m^3) and the optimum moisture content (w_{opt}) was found to be 16.2%.

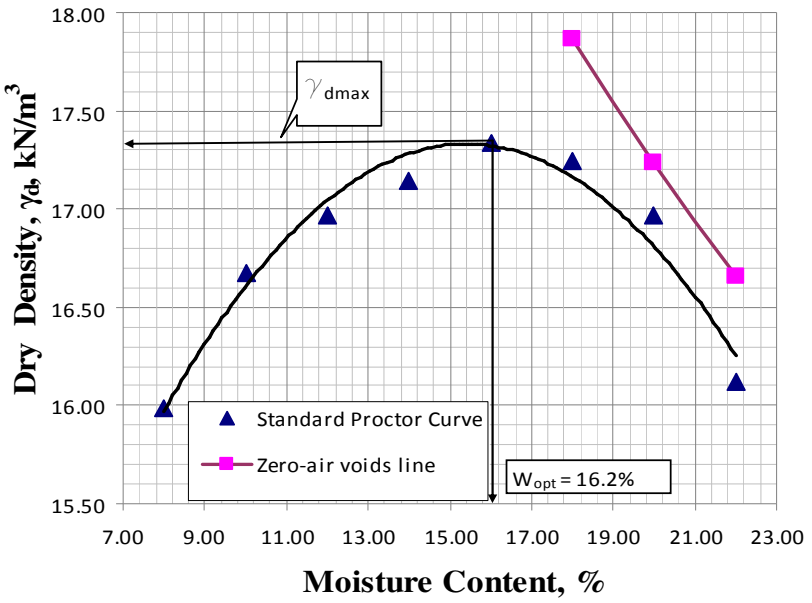

FIG 3.1(b): Standard proctor curve of the soil

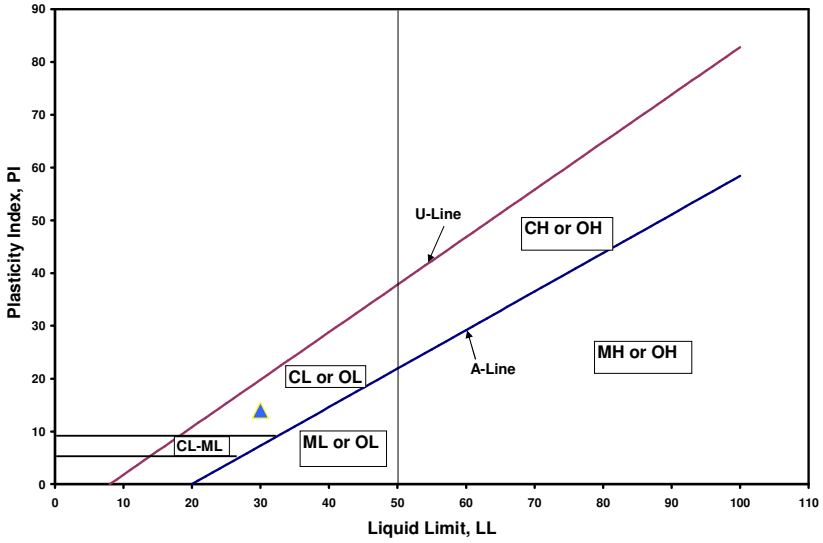

FIG 3.2: Classification curve of the soil

3.1.5 Atterberg Limits

Liquid limit, plastic limit and the shrinkage limits are values predicting the influence of moisture content on soil behavior. These tests are named after Dr. Alfred Atterberg and are carried out on soil particles passing the 425 µm sieve. The tests were performed according to ASTM 4318-05

and the liquid limit was found to be 30 % and the plastic limit 16%. The difference between the liquid limit and the plastic limit is the plasticity index, PI. The PI of the soil was found to be 14. PI is a dimensionless quantity used for classifying fine grained soils. Classification of the soil is shown in Figure 3.2.

3.1.6 Consolidation Test

Consolidation test were performed done on unsaturated soils in the laboratory using a 1-D consolidation apparatus. The maximum pre-consolidation pressure of the soil was determined using the Casagrande's method and was found to be 96kPa. The consolidation curve is shown in Figure 3.3.

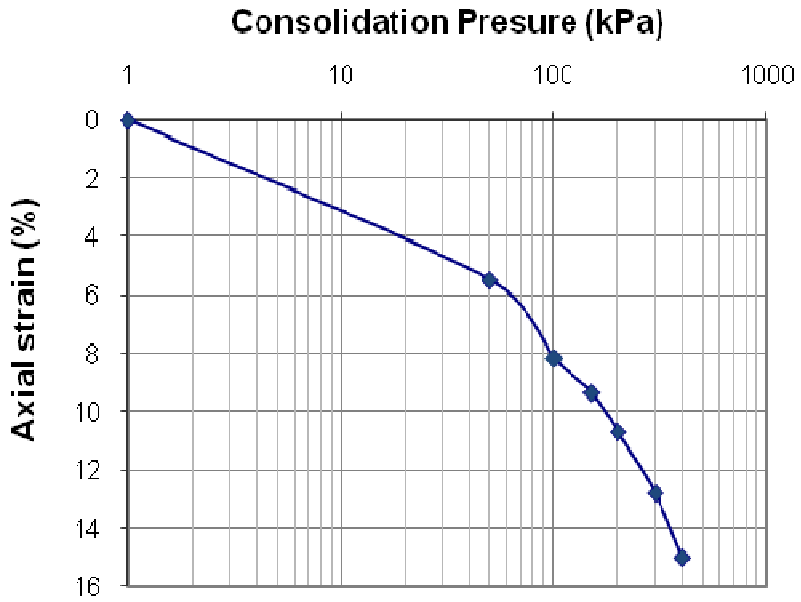

FIG 3.3: Consolidation curve of the soil

3.2 Triaxial Test Specimen Size

Triaxial specimens are normally in a height to diameter ratio of 2:1. The specimen tested had a diameter of 3.8 cm and height of 7.6cm. This type of specimen is not suitable for shear wave measurements because the P-waves or the longitudinal waves travel faster than the S-wave and hence, they arrive first at the receiver bender element making it difficult to predict the exact travel time of the S-wave across the specimen. According to Lee and Santamarina (2005), the

specimen is designed in such a way that the radius (R) to the length (L) of the specimen between the bender elements satisfies Equation 3.1.

$$R \geq \frac{L_s}{2\sqrt{(1-2\nu)}} \tag{3.1}$$

Where, ν is the poisson's ratio and for soils the poisson's ratio ranges between 0.1 and 0.3 and hence the specimen is prepared according to the dimensions specified in Equation 3.1 for evaluating the small strain stiffness (G_{max}) of the soil along the wetting-drying paths of the soil and along the compaction curve. Different specimen sizes were adopted for different tests performed and the sizes of the specimen are mentioned during the explanation of the test configuration.

3.3 Initial Equalization of the Specimen Used in the Drying Test

The specimen for the soil water characteristic curve determination is trimmed out of the extract of the standard proctor test with moisture content at the optimum of 16.2%. The specimen size was 2.5 inches x 2.1 inches. This dimension was adopted so as to improve the clarity of the signals received when using bender elements and also to reduce noise and near-field effects.

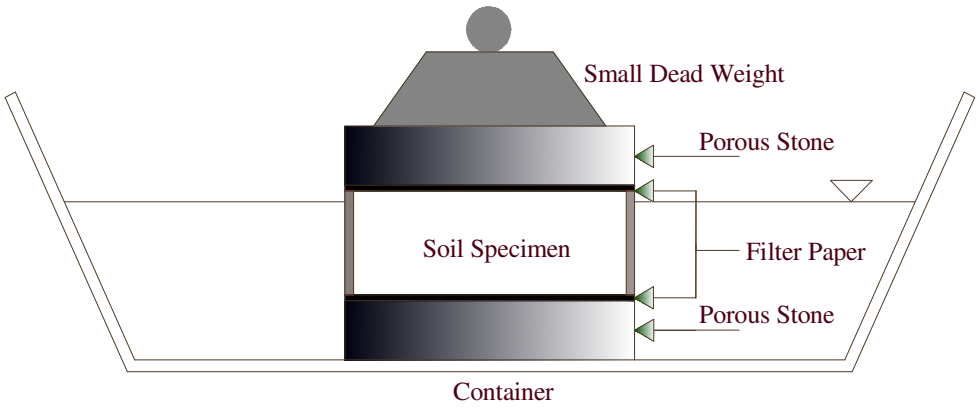

FIG 3.4: Equalization of the soil specimen

The specimen mold was cleaned on the surface and two Whatman (No: 42) filter papers were placed on top and bottom of the specimen as shown in Figure 3.4. This arrangement was kept on a porous stone in a container and the top of the specimen was also covered with a porous stone. De-aired water was then poured in the container until some space was left for air to be let

out of the top of the specimen. A small weight of nearly 50 grams was placed on top of the specimen so as to increase the water content of the specimen. The specimen was immersed for 24 hours before being used to determine the drying curve of the soil.

3.4 Saturation of the High Air-Entry Ceramic Stone

Saturation of the high air-entry ceramic stone was performed similar to the procedure proposed by Fredlund and Rahardjo (1993). The stone is used for measurement and control of the pore water pressure. The stone is assembled in a metal casing ring with epoxy coated all around for making good adhesion. The stone is then saturated before placing any specimen over it. Boiling the stone in water may send the air out from the stone but it might affect the epoxy coating or even create fine cracks in the stone.

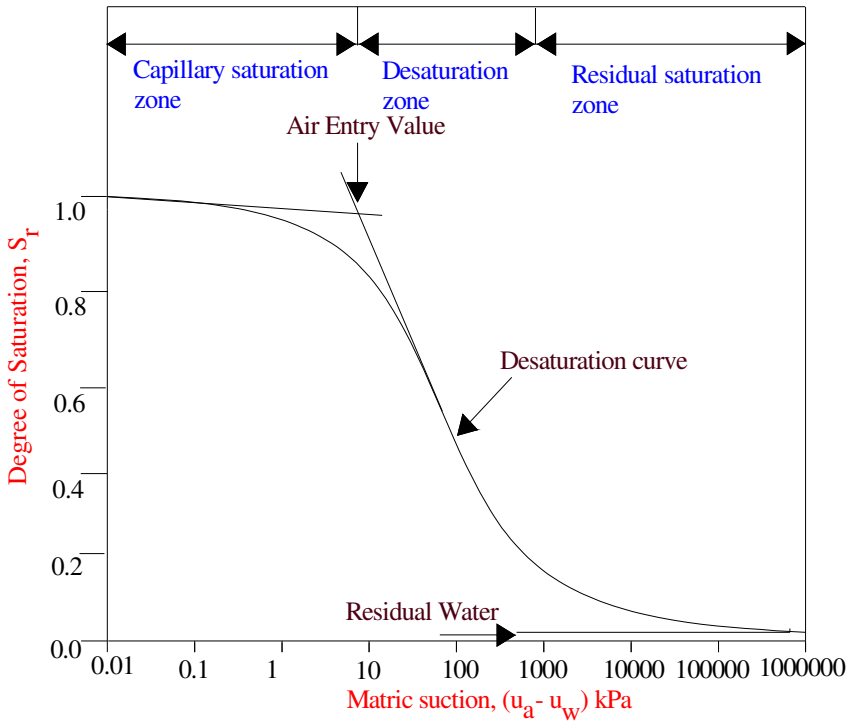

FIG 3.5: Different zones in the soil water characteristic curve

The stone is saturated using a different technique similar to the triaxial cell technique proposed by Fredlund and Rahardjo (1993). The stone is saturated by allowing water to flow

through it and then forcing the air present in the stone to come out eventually. The stone is assembled in the Fredlund's soil water cell without the soil specimen and is filled with water to an inch on top of it. The cell is then subjected to air pressure of 400 kPa and water is allowed to flow through the stone for 1 hour. The air under the stone is periodically flushed and the drainage valves are then closed. The gap under the stone, the stone itself and the cell are all under the same pressure now. The valves are then opened for 10 minutes for water to flow out of the cell and air bubbles are flushed from below the stone. The valves are then closed again and the same procedure is repeated 5-6 times after which the stone should be saturated until it stays in water before putting the specimen on top of it.

3.5 Soil Water Characteristic Curve

3.5.1 Introduction

Soil water characteristic curve (SWCC) is the relationship between the degree of saturation and the matric suction (u_a-u_w). SWCC determines the engineering behavior of unsaturated soils. SWCC is divided into three zones starting at saturation of the soil.

- The Capillary Saturation Zone where the pore-water is in tension and the soil remains saturated due to capillary forces. This stage ends at the air entry value, where the applied suction overcomes the capillary forces and the air enters the soil pores.

- The Desaturation Zone, where water is displaced by the air in the soil pores. This stage ends at residual water content when the pore water becomes occluded and the permeability is greatly reduced.

- The Residual Saturation Zone where the water is tightly adsorbed onto the soil particles and flow occurs in the form of vapor. The soil is almost similar to oven dried soil. When the soil is heated to 105^0C, corresponding to a suction of 1 X 10^6 kPa, it is assumed to

have zero water content. A typical example of the zones of the SWCC is shown in Figure 3.5.

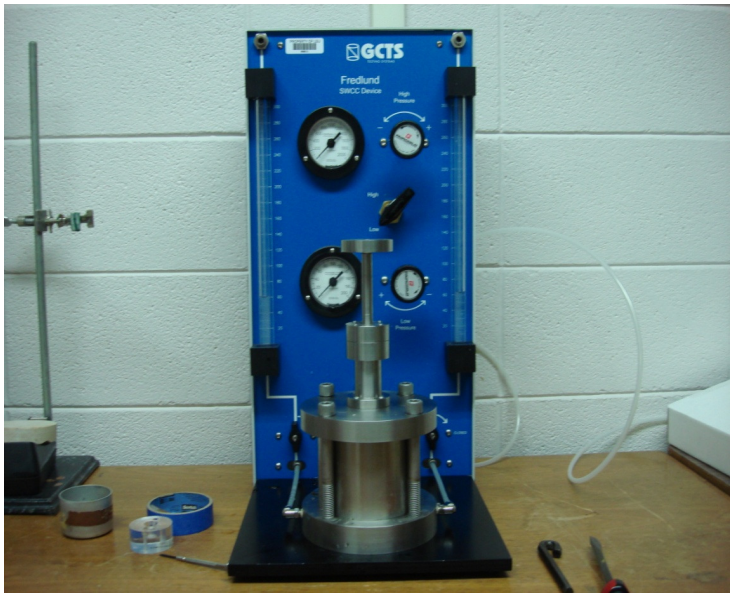

FIG 3.6: A view of the set-up used for determining the soil water characteristic curve used in the laboratory

3.5.2 Methods for Determining SWCC

Soil water characteristics for a particular soil can be determined using several methods available in the literature. Correlation between particle sizes and the soil water characteristics can be used to determine the SWCC of a particular soil. Based on the methods available and the accuracy, laboratory tests seem to give out better results of the SWCC. Volumetric pressure plate extractor, triaxial tests, resonant column devices are common methods of determining the SWCC. All these methods are performed with reasonable accuracy and precision. In this work, we used a Fredlund SWCC device to determine the wetting-drying characteristics of the soil (Courtesy: GCTS Inc.). The method of determining the SWCC is described in the next section in detail.

In this study, the measurement of small strain stiffness (G_{max}) of the soil along the drying

path is to be determined and hence slight modifications to the sample sizes and to the device is done and is discussed in this chapter. The intrinsic properties of the soil are required before computing the soil water characteristic curve of the specimen. The specimen is prepared by trimming out a standard proctor test extract. Once the soil specimen is ready, the following testing procedure is adopted. Each increment of pressure in the drying test is done on a different specimen with the same initial water content. All the readings from different specimens are put together to get the soil water characteristic curve.

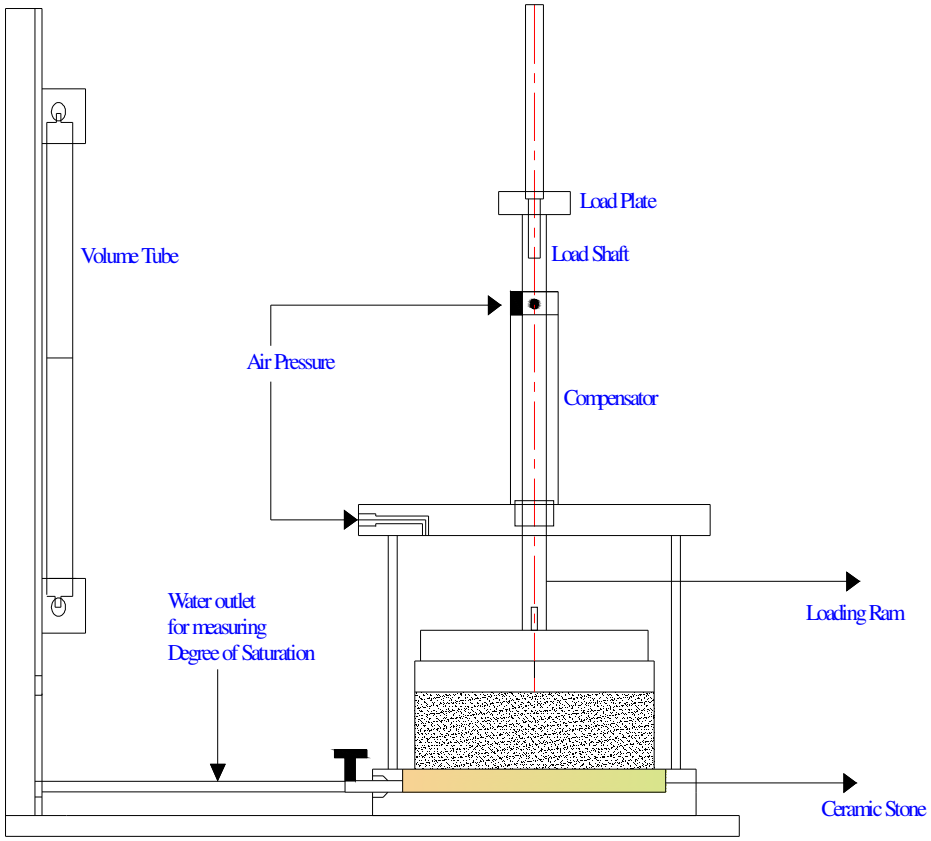

FIG 3.7 Schematics of the instrument for determining the drying curve of the soil

3.5.3 Determination of the Drying Soil Water Characteristic Curve

The specimen was removed from the water and placed on the glass plate without the porous stone and the filter papers. The specimen was allowed to drain out any excess water onto the glass plate and the excess water was removed using a paper towel. The water on the glass plate

and outside the ring was dried. The specimen was weighed along with the glass plate. A 5 bar ceramic stone was selected and saturated as described in the previous sections. The stone was removed and all the excess water was wiped out and weighed. The soil specimen was placed on at the center of the ceramic stone and both the weights were recorded. The SWCC cell assembly was cleaned and assembled with the O-rings and all the fittings as shown in the Figure 3.6 and the schematics are shown in Figure 3.7.

The ceramic stone and the specimen were then pressed at the bottom of the cell and adjusted properly to minimize leakage. Any air under the ceramic stone was removed by the use of a vacuum pump. The loading shaft was then placed over the specimen. The pressure was then applied through two inlets at the back of the top plate (one through the loading shaft and the other through the top plate).

Additional loads could be applied using dead weights or a loading frame. The cell was made air tight by tightening all the screws before the first pressure increment. Any excessive air in the cell was driven out using the vacuum pump. The system was then allowed to equilibrate for some time until the water levels in both the measuring tubes were the same (if different, there might be some more air bubbles below the ceramic stone which were to be removed). The level in the both the measuring tubes were then recorded.

Target pressures were selected and since fine grained soil was tested, pressures of 0, 50,100,200,300,400 kPa were selected to provide a wide distribution of suction values and water contents of the soil. The pressure increment was applied at a rate of 10 kPa/hour (Macari and Hoyos, 2001) to avoid the breaking of the water meniscus around any two unsaturated soil particulates. Target pressures could also be selected based on the D_{60} value (diameter of the particles that represents 60% passing the grain-size distribution curve) or the wPI (weighted plasticity index which is the product of the percent passing no: 200 sieve expressed as a decimal

and the plasticity index) value of the soil. The target pressures could be selected from the family of curves as suggested by Perrera et al, 2005.

The target pressures are selected for an entire range of water content values. The pressure was applied using either the high or low pressure gauge and the corresponding regulator knob was used to apply the pressure in the cell. The pressure compensator will automatically equalize the pressure exerted on the piston from within the chamber. Additional loads could be added on the load plate to simulate the desired total stress or the overburden pressure (p) given by Equation 3.2 and Equation 3.3.

Overburden pressure (p) = Field density X Depth at which the sample is taken. (3.2)

Overburden load = Overburden pressure X Area of the load plate. (3.3)

The system was checked for any kind of leaks using soap water. The system was allowed to equilibrate and the water volume readings are taken on a log-time basis. Readings were recorded before and after flushing air. Equilibration was considered attained once the pressure had been applied for a period of 24 hours and the next pressure increment could be applied when there is no change in the volume of water over a 8-hour period. The time required for equilibration depends on the soil type and the air entry value of the ceramic stone. Highly plastic soils require longer equilibration time. At the end of the final pressure increment, the pressure was released and the soil specimen was weighed and allowed to dry in an oven at 110^0C for 24 hours and the dry weight was recorded. The weight of the surface dry ceramic stone was also recorded and the difference in weights is adjusted in the water volume change readings.

Using the dry weight, the initial water content and the initial dry density were calculated. Using the initial data, the water content corresponding to each pressure increment was calculated. The oven-dried weight was used to calculate the final water content of the sample which provides a check for the test when compared with the data of the last pressure increment.

Disagreement in the water content at the end of the test could be related to an error during the test such as air leak, incorrect data entry, loss of soil during the test or shrinkage of the soil from the confining ring.

3.6 Measurement of Strain

Small strain range of the stress-strain behavior of the soil is highly non-linear and needs a reliable and precise measuring device. External measuring devices such as a linear variable differential transducer (LVDT) could be used to measure axial strains. External strain measurement is prone to errors due to, seating caused by the gaps between the platens, porous stones and the loading ram, alignment errors due to non-verticality of the specimen, non-horizontality of the platens and the tilt of the sample, bedding errors due to surface irregularities and compliance errors. All these errors lead to lower soil stiffness inferred from field observations.

On the other hand, Hall-effect transducers could be used as strain gauges to fix around the specimen and on top and bottom of the specimen. Measurements taken internally show smaller values of axial strains compared to external measurement which shows that the above errors could attribute to the higher value of strain during external measurement. In this study, we do not measure the strain of the soil but we actually measure the shear modulus of the soil using piezo electric transducers and electromagnetic waves which are outlined in the next section.

3.7 Piezo Electric Transducers or Bender Elements

3.7.1 Introduction

Piezo-electric transducers or bender elements are electro-mechanical transducers capable of converting mechanical energy into electrical energy. The elements are made up of two thin piezo-ceramic plates firmly bonded together with brass shim in between. When a voltage is applied to the element, one layer will be in tension and the other in compression resulting in an

electric pulse generated in the elements. The sandwich type mechanism of the element causes one plate to expand and the other plate to contract when voltage is applied. The use of bender elements to measure the small strain characteristics of the soil at very small strains is very simple compared to the conventional triaxial or the resonant column tests with the only disadvantage being the determination of damping ratio of the soil, which can be achieved using resonant column tests. Once the use of the bender elements is known, the determination of the stiffness of soil is very simple compared to the triaxial and resonant column tests.

3.7.2 Preparation of Bender Elements

Bender elements of size 12mm x 5mm x 0.5 mm are obtained. The length of the bender element is parallel to the longitudinal axis of the specimen. Bender elements can be classified as series type and parallel type bender elements which have been discussed in detail in chapter-2. In this research study, we use parallel type bender element, meaning the center shim is exposed at a corner. The two outer plates are properly soldered and a wire is soldered to the center shim such that the soldering lead does not make any contact with the outer layers.

The bender elements have high impedance and hence cannot be exposed to moisture directly. The elements are therefore coated with a water proof polyurethane coat to avoid short circuits. Care must be taken that there is no exposed surface or no air bubbles present in the coat. The coated bender elements are then placed in a slot in the top cap and bottom pedestal which are 1 inch in height and 2.5 inches in diameter, similar to the specimen diameter. The bender elements protrude by about 6mm from the cap and the pedestal. The slot is then filled with epoxy resin to make it air tight and should be free from air bubbles.

The coat is allowed to dry for 24 hours and the bender elements are available for testing now. With this sort of configuration, the bender elements acts as a cantilever beam with the tip moving perpendicular to the length of the specimen causing the soil particles to disorient in the

same direction producing shear waves in the specimen propagating along the length of the element. The top and the base platens are then assembled on top and bottom of the specimen similar to the one shown by Dyvik and Madshus (1985). The bender elements and the top and end platens are shown in Figure 3.8.

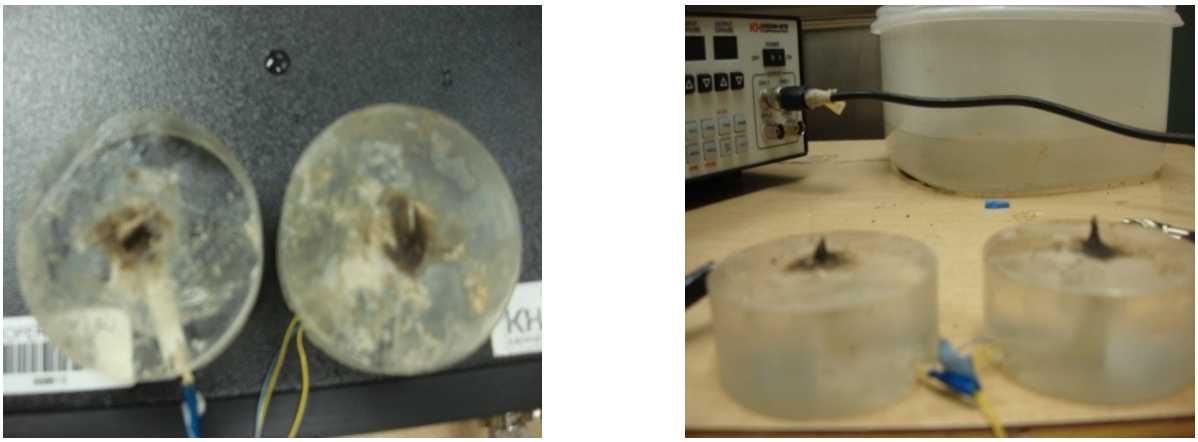

FIG 3.8: Top and bottom platens with protruding bender elements (Parallel type)

3.7.3 Experimental Set-up

In this research, we compute the stiffness characteristics of the soil along the drying path of the soil using a specially designed Fredlund SWCC device and a specially designed triaxial cell for unsaturated soils. We determine the wetting SWCC using the triaxial cell for unsaturated soils as the Fredlund SWCC device is not suited to determine the wetting curve. We also determine the stiffness along the compaction curve of the soil specimen at various different moisture contents along the curve.

3.7.3.1 Instrumentation and Equipments

A Krohnhite 1450 is used as a function generator used in generating the signals. A single sinusoidal pulse was generated and routed into the bender elements and was also sent to one of the four input channels of the Agilent Oscilloscope 6400 series. This signal would trigger the analyzer to start recording the transmitted and received signals. The bottom bender element acts

as a transmitter and the top bender element acts as a receiver. The electric signal generated is converted into mechanical energy by the bender element and is transmitted in the form of vibrations generating shear waves in the soil. The received signal is weak and hence fed to a signal amplifier to amplify the signal suing a Krohnhite 4300 signal amplifier.

(a) **(b)** **(c)**

FIG 3.9: Instruments used to generate and measure signals. (a)Agilent 6014 A Oscilloscope (b) Krohnhite 3944 Signal Amplifier (c) Krohnhite 1400 Function generator

The amplified signal is sent to another channel of the oscilloscope for analysis. The measurements are done using Microsoft excel sheets giving a plot between the voltage on the y-axis and the time on the x-axis. The transmitted and received signals are plotted below each other respectively for easy detection of the travel time. The analysis of the travel time is discussed in the following sections. Figure 3.9 shows the oscilloscope, function generator and the signal amplifier for reference.

FIG 3.10: Experimental set-up showing the specimen with end platens

The bender element transmitter is mounted on the bottom base pedestal, whereas, the bender element receiver is mounted on the top platen. Cylindrical soil sample with height to diameter ratio of 1: 0.6 is placed in the cell on top of the bottom platen, and then the top platen is lowered slowly until it contacts the soil sample.

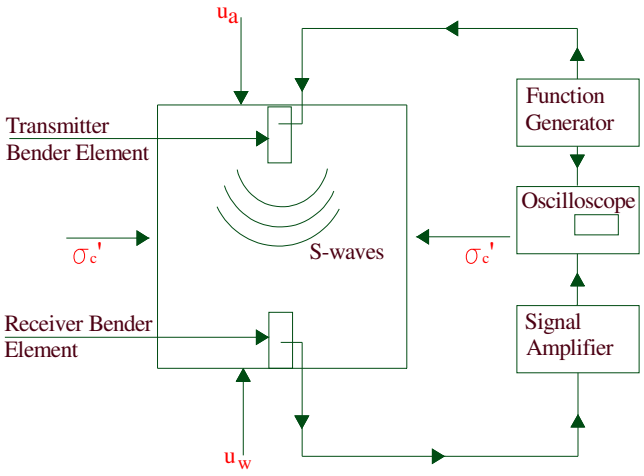

FIG 3.11 : Bender Element test setup (Leong et al, 2005)

The general arrangement of the soil specimen removed from the SWCC cell for determination of the shear wave velocity is simple and is shown in Figure 3.10. The typical procedure of sending the waves and analyzing them is shown pictorially in the form of a flow chart in Figure 3.11.

3.7.3.2 Typical Test Program

The test program was chosen for the following objectives:

- To identify the soil stiffness – shear wave relationship.
- To analyze the influence water content and percentage of fines in the specimen in determining the shear wave velocity.
- To analyze the arrival time of the wave.

To achieve these objectives, the soil sample was subjected to values of suction ranging

between 0 and 400kPa in the Fredlund's SWCC cell and the triaxial cell. The shear wave velocity was calculated at and after each pressure increment in the SWCC cell whereas, it is a continuous measurement in the triaxial cell. The peak-to-peak energization voltage used to drive the bender elements was 20 V in this study and a frequency ranging for 5-10 Hz was found optimum. The procedure involving the measurement of shear wave velocity is rather simple and easy to perform than the conventional triaxial tests.

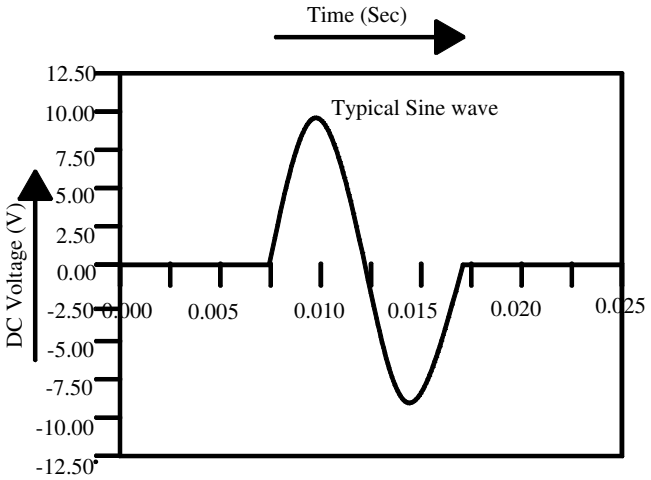

FIG 3.12: Typical transmitted sine wave pulse

The input voltage from a function generator is sent into the trasmitter bender element in the form of a pulse sine wave signal in the Figure 3.12 causing the vibraton in the element. The receiver element receives the signal. The input signal and the received signal are identified using an oscilloscope and the time taken for the signal to pass through the sample is recorded. The received signal might be weak due to many reflections in the cell and hence, an amplifier is used to amplify the signal.

Shear wave velocity, V_s is calculated according to Equation 3.4,

$$V_s = \frac{L}{t_s} \tag{3.4}$$

Where, t_s are obtained either by manual or by correlation methods described above, and L is the current effective height of soil sample (tip to tip distance between the bender elements). Tip to tip distance is considered because the soil particles surrounding the bender elements are likely to get disturbed due to the small perturbations in the bender element while transmitting the signal.

The results for the shear wave velocity are discussed in the next chapter. The small strain shear modulus of the soil (G_{max}) could be calculated using Equation 3.5,

$$G_{\max} = \rho V_s^{\,2} \tag{3.5}$$

Where, ρ is the bulk density of the soil and V_s is the shear wave velocity.

3.8. Analysis of Travel Time

Due to the distortion of the wave during its passage through the soil specimen, four methods have been suggested for the determination of travel time, "t" (Viggiani and Atkinson, 1995a). Figure 3.12 shows an example of a received signal.

- ***First arrival time*:** First arrival time is defined as the travel time to the first arrival of the receiver signal (may be first deflection point or the first reversal point).
- ***Travel time between characteristic points***: Characteristic peaks correspond to the time for the start of the transmitter signal to the first peak of the received signal (Viggiani and Atkinson, 1995a).
- ***Cross-correlation of input and output signals***: Cross-correlation is the travel time taken as the time shift that produces a peak correlation between the input and output signals.
- ***Cross-power of transmitter and receiver signals***: Cross-power is the time difference between the characteristics of the transmitter and the receiver when they are interchanged. The following figure shows a representative step sine wave signal and the different points of arrival time based on the analysis of different researchers.

From Figure 3.13, we arrive at the following conclusions regarding arrival time;

- Point A is considered as the first arrival based on S-wave polarization or in process monitoring. (Fam and Santamarina,1995)
- Point B is adopted when there is a sudden jump. (Dyvik and Madshus, 1985).
- Point C or a Point between B and D has been suggested from comparisons with input sine signals, cross-correlation analyses or on the basis of testing specimens of different height. (Kawaguchi et al. 2001).

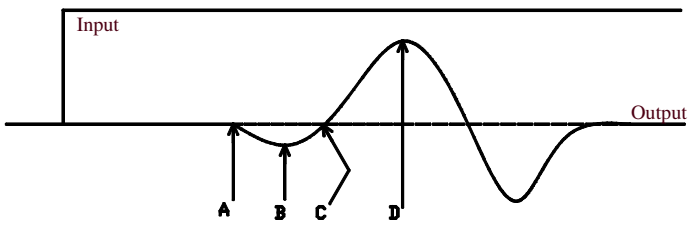

FIG 3.13: Typical example of a received S-wave signal.

Figure 3.14 shows the process of determining the time taken by the signal to complete one cycle of motion for the transmitter to the receiver bender elements. In this research study, we consider characteristic peaks method to determine the travel time. We also consider the first point (Point B) of action of the wave and check this value to be close or equal to the characteristic peaks.

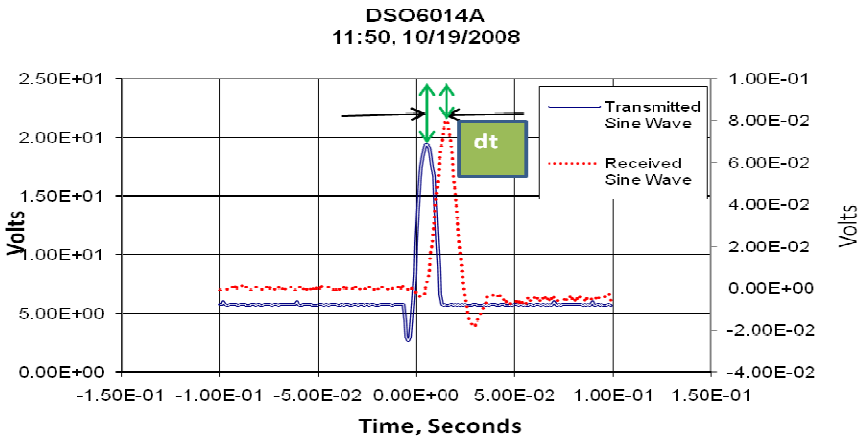

FIG 3.14: Time delay by characteristic peak point method

3.9 Errors Associated with Set-up

- Reflections and refractions of the wave due to the finite sample size
- The principal problem with this method has always been the subjectivity of the determination of the arrival time.
- Typically used square wave is composed of a spectrum of different frequencies.
- From the received trace of the square wave alone, it is uncertain of the first point of arrival of the shear wave.

Viggiani and Atkinson (1995a) attempted to reduce the degree of subjectivity in the interpretation, they suggested the use of a sine pulse which only had a single pulse and which could reduce the error by about ±7%. In this research study, a sine wave pulse is used in determining the shear wave velocity of the soil and in calculating the small strain stiffness (G_{max}) of the soil. Tests in determining the stiffness along drying path, stiffness along the compaction curve at different water contents and stiffness of an unsaturated triaxial specimen along the wetting-drying paths are the main features of the study.

3.10 Determination of Soil Stiffness Using Unsaturated Triaxial Cell

To minimize the errors from the previous testing techniques and to check the experimental test results obtained for the drying curve of the soil, the measurement of soil stiffness was done using a triaxial specimen with a diameter of 50mm and 100mm in height. For the effective arrival of the shear wave, the sample size was reduced to 42 mm once the soil was subjected to a specific value of suction. This height was used to enhance the arrival of the shear wave or the S-wave before the longitudinal wave or the P-wave.

The triaxial cell was a special double walled cell capable of handling pore-air and pore-water pressure separately through different inlets. The end platens of the specimen have two filters each with a high air entry filter capable of withstanding a pressure up to 1500kPa and a

low air entry filter used for application of pore-air pressure. The bottom end platen is fixed to the bottom of the cell so as to minimize the specimen movements and also minimizing the lateral distortion of the specimen. The experimental set-up of the specimen is shown in Figure 3.15.

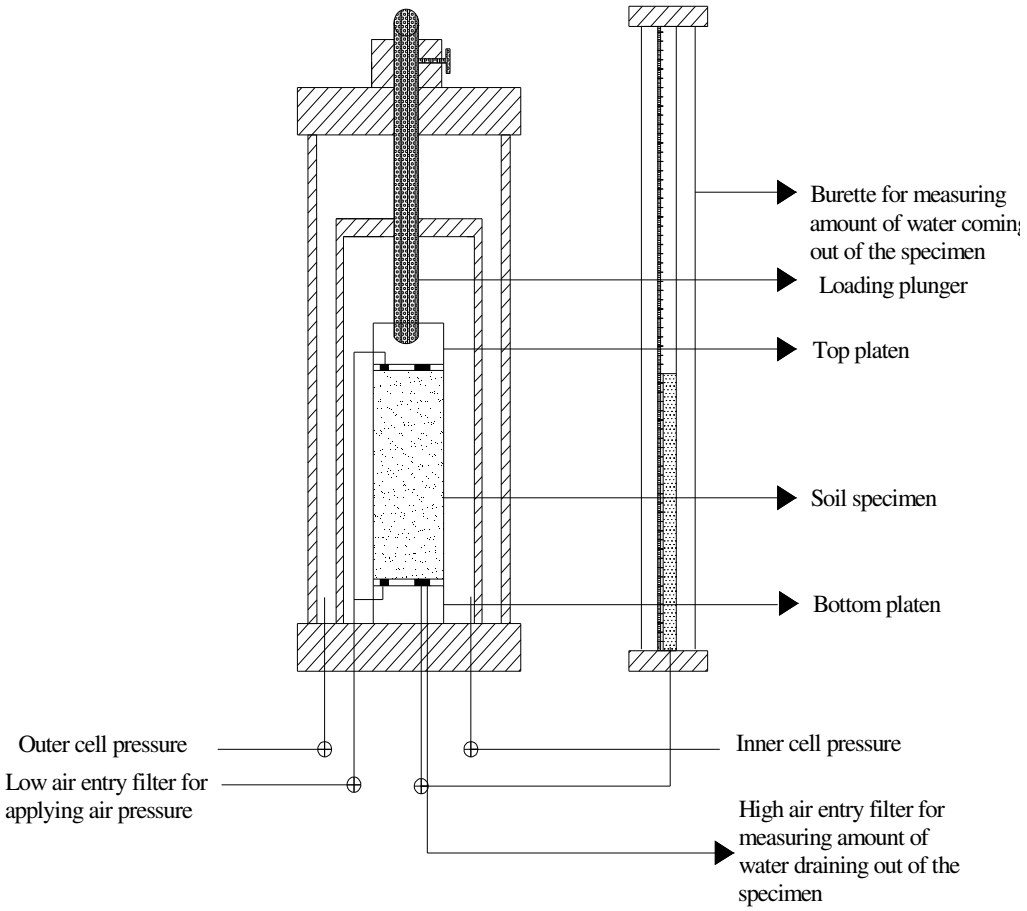

FIG 3.15: A view of the experimental set-up of the unsaturated triaxial system

3.10.1 Saturation of the High Air-Entry Filters

The purpose of the high air-entry filter is to allow water to pass through it and to stop air from doing so. Hence for accurate measurements of the amount of water flowing in and out of the soil it is absolutely necessary to saturate the stone.

The saturation of the high air-entry filter is similar to the procedure proposed by Fredlund and Rahardjo (1993). The bottom platen is fixed to the bottom of the cell and the interior and the exterior cell are filled with water until over 2 inches above the platen. The outer and the inner

chambers are pressurized to the same pressure so as to minimize the expansions of the perspex used to prepare the cell. The chamber was pressurized to a pressure of 600 kPa with the outlet drains of the high air-entry filter closed.

The pressure was applied for an hour and at this point, all the corners of the filter were at the same pressure. The drains were opened for 10 minutes after an hour to allow the pressurized air bubbles to flow out of the filter and then the drains were closed again. This procedure was repeated 6 to 7 times and when no air-bubbles were seen gushing out the stone was assumed saturated. The low air-entry filter need not be saturated because its main purpose is to allow the flow of air through the soil.

It was not possible to saturate both the platens at the same time and hence it was decided not to use the top high air-entry filter to measure the flow of water in and out of the specimen but the low air entry filter was used to apply air pressure on top of the specimen.

3.10.2 Specimen Preparation

The soil specimen was prepared after compaction in a standard proctor mold at +2% wet of the optimum moisture content and then trimming and sizing the extract of the specimen as shown in Figure 3.16. The water content was adopted so as to ease the trimming and sizing procedure of the specimen. The extract from the standard proctor mold was cut into two equal halves so as to facilitate in trimming the specimen exactly to a diameter of 50mm. Specimen trimming was done with the help of a wire saw with the specimen places between two pedestals of diameter 50mm as shown in Figure 3.16. The top pedestal was fixed and the bottom one was free to rotate so as to position the specimen for trimming.

The trimmed specimen was 50mm in diameter and 100mm long. The specimen was then made to stand over the triaxial end platens with the help of an elastic membrane. Care was taken that the platens rested exactly on top of the specimen without any lateral movement, thereby

causing any distortion to the specimen. The top and bottom platens were then sealed with o-rings so as to disallow the specimen from directly coming in contact with the cell pressure applied.

FIG 3.16: Triaxial specimen preparation from a standard proctor extract

3.10.3 Unsaturated Triaxial Testing Procedure

The specimen was mounted in the cell and the low air-entry filter of the top and bottom platens were connected with the help of a t-connection to a pressure regulator which was connected to the air-line. The air line had a maximum pressure capacity of 600 kPa but all the tests performed were at a maximum pressure of 400kPa and hence proved to be sufficient. The main difference in using the triaxial procedure and the Fredlund's SWCC procedure is that, in the triaxial test the sample is subjected to pressure from all the sides whereas in the Fredlund's test, the soil is compressed from the top and constrained by a confining ring laterally.

The inner and the outer chambers of the cell were then filled with de-aired water so as to minimize squeezing of the specimen due to sole air-pressure application. Care was taken that the pressure applied through the low air-entry filter and the cell pressures were the same so as to avoid bulging of the membrane from the inside and also all our tests were performed at isotropic

stress conditions and hence this set-up proved satisfactory.

The drain of the bottom high air-entry filter was connected to a burette so as to measure the amount of water flowing out of the specimen (drying) and flowing into the specimen (wetting). Cell pressure of 0, 100, 200, 300, 400 kPa were applied to the specimen with the pressure increment given at 10 kPa per hour.

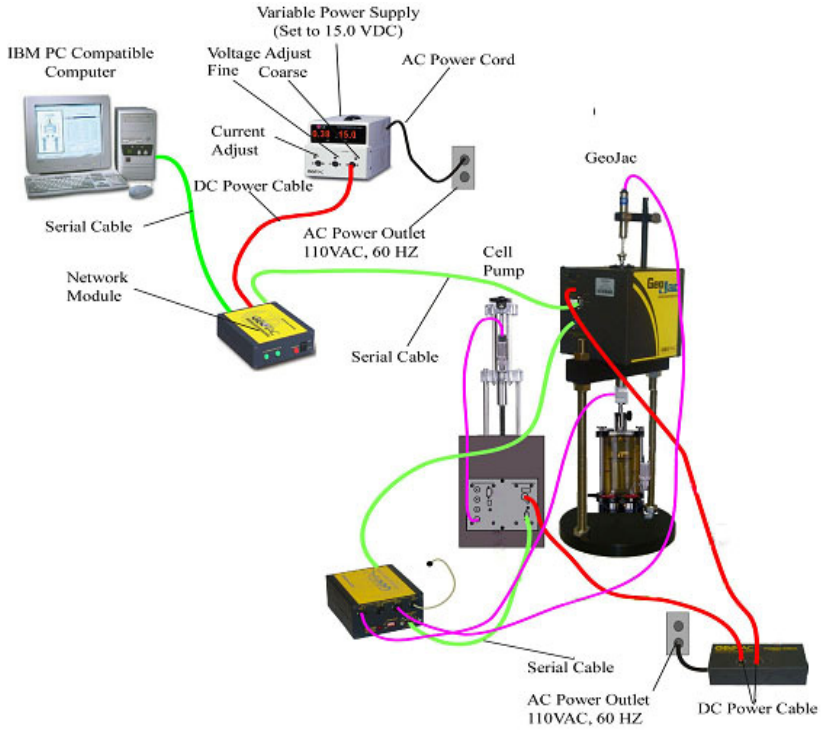

FIG 3.17: Connections of the unsaturated triaxial device (Courtesy: GeoTAC Inc.)

Each pressure was applied for 24 hours for drying and 24 hours for wetting by reducing the pressure to 100 kPa less than the value at the rate of 10 kPa per hour. Hence, a minimum of 5 test specimens were required to complete the whole set of pressure increments at least once and to plot the wetting- drying curve of the soil. Before the beginning of the test, the weight of the sample was taken so as to determine the initial water content and also the weight was taken after the test to determine the final water content. The calculations and the results obtained are presented in chapter-4 and the details of the results are given. The line diagram showing all the

connections is shown in Figure 3.17 and labeled for immediate understanding of the reader and the experimental set-up in the laboratory is shown in Figure 3.18.

FIG 3.18: Experimental set-up of the unsaturated triaxial device in the laboratory

3.10.4 Measurement of Stiffness

The measurement of stiffness was done after the pressure increments were completed for a cycle of wetting-drying of the soil. The specimen was removed from the cell and weighed for its water content and then was connected with bender elements attached to two platens with the top as the transmitter and the bottom platen as the receiver shown in Figure 3.9. Measurements were done on each and every sample and the results were plotted to determine the hysteresis (w %) similar to the hysteresis of unsaturated soils along the wetting-drying paths as proposed by Wheeler et al., 2001. The results have been shown in chapter-4 for any further reference. It was important to measure the stiffness as soon as the test was completed so that there would be no effect due to evaporation on the sample and the value of the stiffness of the soil. This chapter explains all the soil properties obtained and the procedures to perform all the experiments proposed in this research study with the figures and equations wherever necessary.

CHAPTER 4 EXPERIMENTAL RESULTS

4.1 Introduction

Experimental results are presented in this chapter from the various types of tests performed. Drying curve obtained from 1-D soil water characteristic curve device is presented along with the variation of stiffness along the drying curve. Variation of compacted soil stiffness to moisture content, consolidation pressure and undrained shear strength is also presented. Wetting drying curves were determined using an unsaturated triaxial device and their results are shown. Soil water characteristic curves were plotted with the water content against matric suction and the stiffness was found to be higher on the wetting side than for the same value of matric suction on the drying side.

4.2 Relationships for Determining Small Strain Shear Modulus (G_{max})

The mechanical behavior of unsaturated soils is governed by the net normal stress and the matric suction and along the polarization plane. Yuen (2004) proposed an empirical relationship to express the shear wave velocity (V_s) according to the two stress state variables shown in Equation 4.1. He conducted different experiments on compacted and intact specimen and studied the anisotropic variation of stiffness along the wetting and drying paths of unsaturated soils.

$$V_{s(ij)} = C_{ij} f(e) \left[\frac{\sigma_i - u_a}{p_r} * \frac{\sigma_j - u_a}{p_r} \right]^{n/2} \left[1 + \left(\frac{u_a - u_w}{p_r} \right) \right]^{b_{ij}} \tag{4.1}$$

where, b_{ij} is an exponent of matric suction (u_a - u_w) showing the influence of matric suction on the shear wave in the polarization plane ij, p_r is the reference pressure typically equal to 1 kPa, C_{ij} is a soil fabric constant, f (e) is a function of void ratio and (σ_i - u_a) and (σ_j- u_a) are principal effective stresses in the plane of the shear wave with n as a component of the effective stress. The isotropic variation of the shear wave velocity is represented by Equation 4.2.

$$V_{s(ij)} = C_{ij} f(e) \left[\frac{\sigma_i - u_a}{p_r} \right]^n \left[1 + \left(\frac{u_a - u_w}{p_r} \right) \right]^{b_{ij}} \quad (4.2)$$

When matric suction is zero (u_a-u_w = 0) in Equation 4.1 and Equation 4.2, it represents saturated soils. Equation 4.1 is used when the shear wave velocity is to be measured in more than one plane of polarization and hence, is not significant in this study. In this research study, we analyze the variation of the small strain shear modulus (G_{max}) along the longitudinal axis (length) of the specimen.

The strain induced by the use of bender elements to the soil is less than 0.001% and hence considered elastic. The velocity of the shear wave (S-wave) is a function of the length of the specimen and the time taken by the transmitted wave to traverse one length of the specimen to reach the receiver bender element. The velocity of the shear wave (V_s) is determined the following Equation 4.3,

$$V_s = \frac{L_s}{t_s} \quad (4.3)$$

where, t_s is the propagation time of the shear wave and L_s is the length of the specimen.

The small strain shear modulus (G_{max}) is determined by Equation 4.4 and is the important parameter related to the stiffness of the soil. The density of the soil is the density at the optimum moisture content as all the samples are prepared at this moisture content.

$$G_{\max} = \rho V_s^{\,2} \quad (4.4)$$

where, ρ is the bulk density of the specimen which is a function of the degree of saturation (S_r), void ratio (e), the specific gravity (G_s) and the density of water (ρ_w) determined by Equation 4.5.

$$\rho = \frac{G_s + S_r e}{1 + e} \rho_w \quad (4.5)$$

The tests to determine the stiffness are conducted assuming that the soil is isotropic and the failure in shear and the small strain shear modulus (G_{max}) represents the shear stiffness of the soil. In this study, we do not analyze the degree of anisotropy of the soil which is a true fact since the stiffness of the soil in one plane is not equal to the stiffness in any other plane.

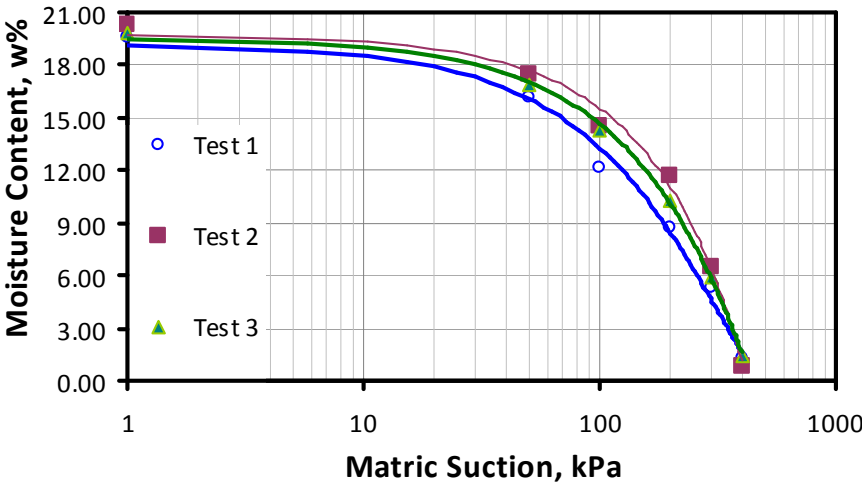

FIG 4.1 : Soil water characteristic curve of the soil along the drying side

4.3 Experimental Results of Stiffness (G_{max}) from the Drying Tests in the GCTS Cell

4.3.1 Soil Water Characteristic Curve

A total of three tests were performed on the soil for each pressure increment with the difference between the readings being less than 5% are plotted and the figures are shown in this section. The soil in the GCTS cell is subjected to air pressure ranging from 0-400 kPa on the surface of the specimen and is confined to the ring laterally. The soil specimen hence undergoes a process of one dimensional compression due to the air pressure causing the release of water from the soil pores. The pressure in the cell is increased at a rate of 10 kPa/ hr (Macari and Hoyos, 2002) to avoid breaking of the meniscus causing variation in the mechanical behavior of the soil. Each pressure increment is applied for 24 hours on the soil allowing the soil to equilibrate and the next pressure increment is given when there is no change in the water coming out of the soil for a

period of 8 hours. After each pressure increment was applied, the soil specimen was removed and checked for moisture content and the measurement for shear stiffness was made immediately after being removed right outside the cell using bender elements.

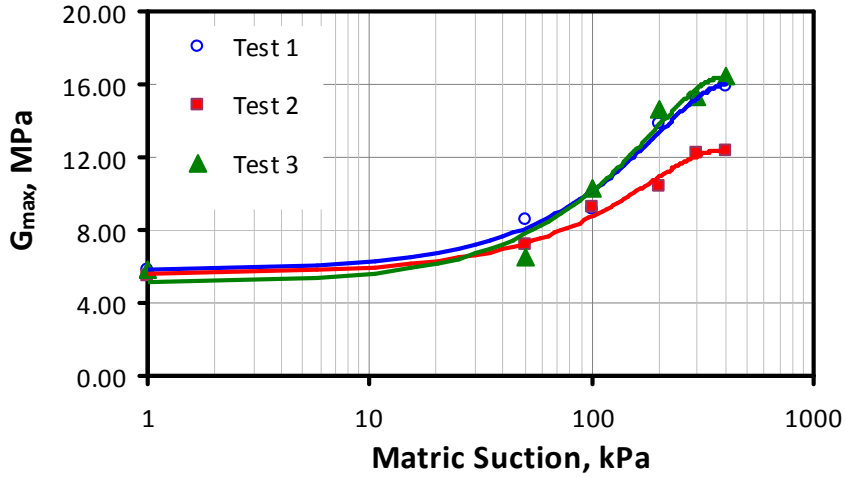

(a)

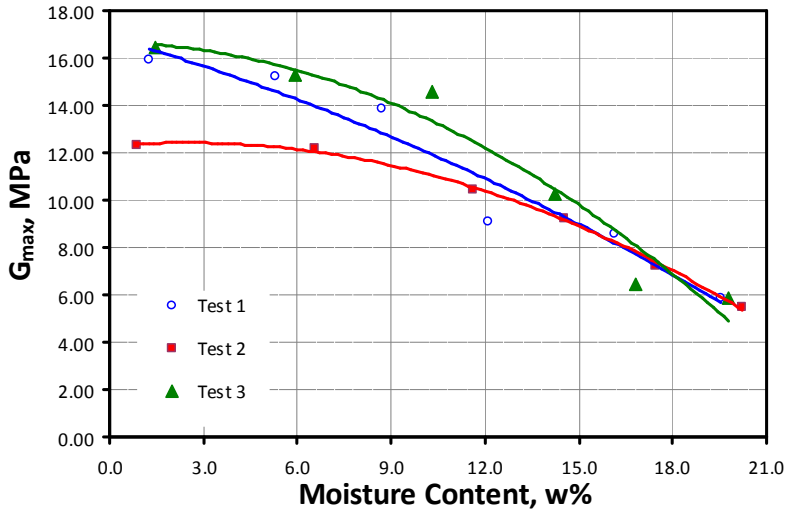

(b)

FIG 4.2(a) and (b): Variation of small strain stiffness (G_{max}) with matric suction (u_a-u_w) and moisture content (w %)

The drying soil water characteristic curve for the specimen is shown in Figure 4.1. It was observed that there is not a significant change in the water content until the soil reaches its air entry value and after that the water content decreases drastically meaning the loss of the capillary and the inter-particle forces during this phase of the curve. The air entry value of the soil was

found to be close to 80kPa which can be found out from the curve in Figure 4.1. Figure 4.1 suggests that with an increase in matric suction, there is a non-linear increase in soil stiffness along the drying path of the soil similar to the results shown in Figure 2.6 proposed by Mancuso et al. (2002) who measured the soil stiffness using a resonant column device. Triaxial tests were performed to determine the wetting soil water characteristic curve of the soil.

The shear wave velocity of the soil is measured outside the cell the GCTS cell. Once a desired pressure increment is achieved, the soil specimen is taken out and the bender elements are installed on top and bottom of the specimen to measure the time taken by the shear wave to traverse the length of the specimen. The procedure is clearly discussed in Chapter 3 for reference. The variation of the small strain shear modulus (G_{max}) with the soil matric suction and the water content (w %) is shown in Figure 4.2(a) and Figure 4.2(b) respectively.

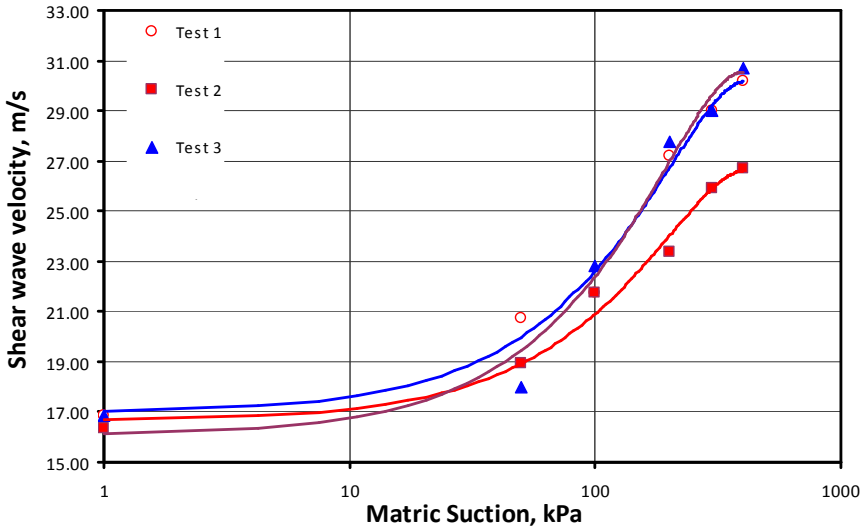

FIG 4.3: Variation of shear wave velocity (V_s) with matric suction (u_a-u_w)

The results suggest that there is an increase in the stiffness of the soil with increase in soil suction also suggesting the non-linearity of the behavior of stiffness with soil matric suction (Atkinson, 2000). The small strain shear modulus of the soil (G_{max}) decreases with an increase in the water content (w %) of the soil with the decrease as significant as 65% to the shear modulus

at 0 kPa suction. The variation of the shear wave velocity with soil matric suction is presented in Figure 4.3.

Tests were also conducted on specimens prepared from the modified proctor test. The drying curve can be seen in Figure 4.4(a) and the stiffness curve in Figure 4.4(b). The air entry value of the soil was found to be close to 90 kPa and the shear stiffness was found to increase with increase in compaction energy but increases with soil matric suction similar to the specimens prepared from the standard proctor test.

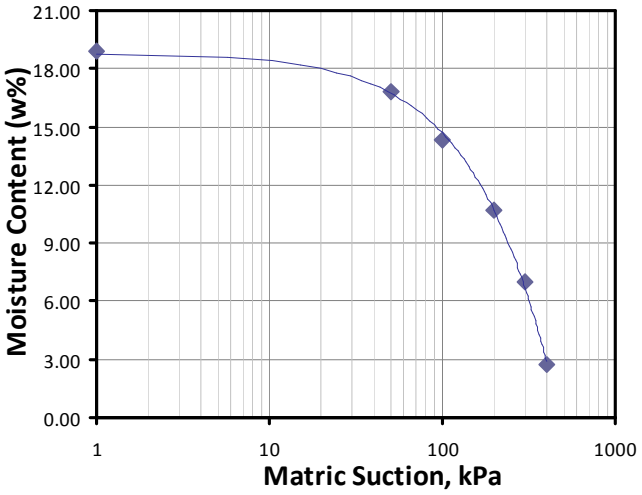

(a)

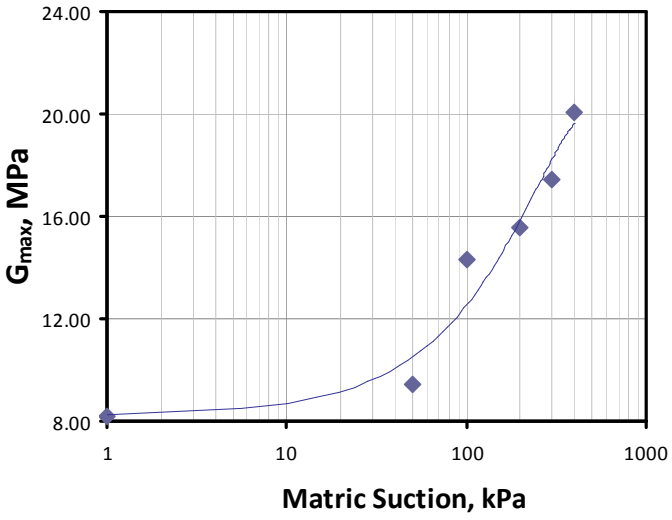

(b)

FIG 4.4: (a) Drying curve for modified proctor sample (b) Drying stiffness curve for modified proctor sample

TABLE 4.1 (a): Calculation of results from the GCTS cell – Test 1

Specific Gravity	G_s	2.71	
Weight of dry soil	W_s	322.00	g
Volume of ring	V_r	183.39	cc
Weight of ring	W_r	375.00	g
Volume of dry soil	$V_s = W_s/G_s$	118.82	cc
Volume of Voids	$V_v=V_r-V_s$	64.57	cc
Void Ratio	$e=V_v / V_s$	0.54	
Specific Volume	$\nu=1+e$	1.54	
Dry Density	$\rho_{dry} = W_s/V$	1.76	g/cc
Density	$\rho=\rho_{dry}*(1+w)$		
Length between BE		5.80	cm

Suction	**Weight of Wet soil**	**Weight of Water**	**Water Content**	**L**	**R**	**Water released**	**Projected Weight**	**Density**	**Time**	**V_s**	**G_{max}**
kPa	**g**	**g**	**%**	**ml**	**ml**	**ml**	**g**	kNs^2/m^4	s	m/s	MPa
1	385	63	19.57	151	151	0	385	20.60	0.00344	16.86	5.85
50	374	52	16.15	157	157	10	375	20.01	0.00280	20.71	8.58
100	361	39	12.11	163	163	12	363	19.31	0.00267	21.72	9.11
200	350	28	8.70	170	170	12	351	18.72	0.00213	27.23	13.88
300	339	17	5.28	179	179	14	337	18.13	0.00200	29.00	15.25
400	326	4	1.24	187	187	14	323	17.44	0.00192	30.21	15.92

(Table Continued)

TABLE 4.1 (b): Test 2

Specific Gravity	G_s	2.71	
Weight of dry soil	W_s	319.6	g
Volume of ring	V_r	183.39	cc
Weight of ring	W_r	375	g
Volume of dry soil	$V_s = W_s/G_s$	117.93	cc
Volume of Voids	$V_v=V_r-V_s$	65.46	cc
Void Ratio	$e=V_v / V_s$	0.56	
Specific Volume	$\nu=1+e$	1.56	
Dry Density	$\rho_{dry} = W_s/V$	1.74	g/cc
Density	$\rho=\rho_{dry}*(1+w)$		
Length between BE		5.8	cm

Suction	**Weight of Wet soil**	**Weight of Water**	**Water Content**	**L**	**R**	**Water released**	**Projected Weight**	**Density**	**Time**	**V_s**	**G_{max}**
kPa	**g**	**g**	**%**	**ml**	**ml**	**ml**	**g**	kNs^2/m^4	**s**	m/s	MPa
1	384.3	64.7	20.24	143	143	0	384.3	20.56	0.00355	16.34	5.49
50	375.4	55.8	17.46	147	147	8	376.3	20.08	0.00306	18.95	7.21
100	366.1	46.5	14.55	152	152	10	366.3	19.58	0.00267	21.72	9.24
200	356.8	37.2	11.64	157	157	10	356.3	19.09	0.00248	23.39	10.44
300	340.5	20.9	6.54	165	165	16	340.3	18.21	0.00224	25.89	12.21
400	322.4	2.8	0.88	173	173	16	324.3	17.25	0.00217	26.73	12.32

(Table Continued)

TABLE 4.1 (c): Test 3

Specific Gravity	G_s	2.71	
Weight of dry soil	W_s	321.20	g
Volume of ring	V_r	183.39	cc
Weight of ring	W_r	375.00	g
Volume of dry soil	$V_s = W_s/G_s$	118.52	cc
Volume of Voids	$V_v=V_r-V_s$	64.87	cc
Void Ratio	$e=V_v / V_s$	0.55	
Specific Volume	$\nu=1+e$	1.55	
Dry Density	$\rho_{dry} = W_s/V$	1.75	g/cc
Density	$\rho=\rho_{dry}*(1+w)$		
Length between BE		5.80	cm

Suction	**Weight of Wet soil**	**Weight of Water**	**Water Content**	**L**	**R**	**Water released**	**Projected Weight**	**Density**	**Time**	**V_s**	**G_{max}**
kPa	**g**	**g**	**%**	**ml**	**ml**	**ml**	**g**	kNs^2/m^4	**s**	m/s	MPa
1	384.8	63.6	19.80	122	122	0	384.8	20.58	0.00344	16.86	5.85
50	375.2	54	16.81	127	127	10	374.8	20.07	0.00323	17.96	6.47
100	366.9	45.7	14.23	131	131	8	366.8	19.63	0.00254	22.83	10.23
200	354.3	33.1	10.31	137	137	12	354.8	18.95	0.00209	27.75	14.59
300	340.2	19	5.92	144	144	14	340.8	18.20	0.00200	29.00	15.30
400	325.9	4.7	1.46	151	151	14	326.8	17.43	0.00189	30.69	16.42

TABLE 4.2 (a): Calculation of results from the standard proctor test – Test 1

Specific Gravity	**G_s**	2.71	
Wt. of dry soil		311	g
Vol. of ring	**V_r**	200.83	cc
Wt. of ring		375	g
Vol. of dry soil		114.76	cc
Vol. of Voids	**$V_v=V_r-V_s$**	86.07	cc
Void Ratio	**$e=V_v/V_s$**	0.75	
Specific Volume	**$v=1+e$**	1.75	
Dry Density	**$\rho_{dry}=W_s/V$**	1.55	g/cc
Density	**$\rho=\rho_{dry}*(1+w)$**		
Effective Length of the Sample	**Tip to tip distance**	**5.3**	**cm**

Water Content, %	**Time**	**V_s(m/s)**	**ρ (kNs^2/m^4)**	**G_{max}(MPa)**
10.2	0.002	26.50	16.74	11.76
11.53	0.0024	22.08	16.94	8.26
12.2	0.0032	16.56	17.05	4.68
13.66	0.0032	16.56	17.27	4.74
14.2	0.004	13.25	17.35	3.05
15.06	0.0048	11.04	17.48	2.13
16.2	0.0056	9.46	17.65	1.58
17.51	0.006	8.83	17.85	1.39

(Table Continued)

TABLE 4.2 (b): Test 2

Specific Gravity	**G_s**	2.71		
Wt. of dry soil		315	g	
Vol. of ring	**V_r**	200.83	cc	
Wt. of ring		375	g	
Vol. of dry soil		116.24	cc	
Vol. of Voids	**$V_v=V_r-V_s$**	84.59	cc	
Void Ratio	**$e=V_v/V_s$**	0.73		
Specific Volume	**$v=1+e$**	1.73		
Dry Density	**$\rho_{dry}=W_s/V$**	1.57	g/cc	
Density	**$\rho=\rho_{dry}*(1+w)$**			
Effective Length of the Sample	**Tip to tip distance**	**5.3**	**cm**	
Water Content (%)	**Time (Seconds)**	**V_s(m/s)**	**ρ (kNs^2/m^4)**	**G_{max}(MPa)**
10.2	0.002	26.50	16.96	11.91
12.2	0.0032	16.56	17.26	4.74
14.2	0.004	13.25	17.57	3.09
16.2	0.006	8.83	17.88	1.40
18.2	0.0064	8.28	18.19	1.25
20.2	0.008	6.63	18.50	0.81
22.2	0.01	5.30	18.80	0.53
24.2	0.0144	3.68	19.11	0.26
26.2	0.0296	1.79	19.42	0.06

TABLE 4.3: Calculation of results from the modified proctor test

Specific Gravity	**G_s**	2.71	
Wt. of dry soil		371	g
Vol. of ring	**V_r**	200.84	cc
Wt. of ring		375	g
Vol. of dry soil		136.90	cc
Vol. of Voids	**$V_v=V_r-V_s$**	63.94	cc
Void Ratio	**$e=V_v/V_s$**	0.47	
Specific Volume	**$v=1+e$**	1.47	
Dry Density	**$\rho_{dry}=W_s/V$**	1.85	g/cc
Density	**$\rho=\rho_{dry}*(1+w)$**		
Effective Length of the Sample	**Tip to tip distance**	**5.3**	**cm**

Water Content (%)	**Time (Seconds)**	**V_s(m/s)**	**ρ (kNs^2/m^4)**	**G_{max}(MPa)**	**w%**	**ρ_d (kN/m^3)**
11.3208	0.00172	30.81	20.17	19.15	11.50	17.95
12.1294	0.00200	26.50	20.32	14.27	12.42	18.33
13.2075	0.00213	24.88	20.51	12.70	13.21	18.59
14.2857	0.00267	19.85	20.71	8.16	14.70	18.68
15.0943	0.00291	18.21	20.86	6.92	17.95	16.55

4.4 Experimental Results of Stiffness (G_{max}) along the Compaction Curve

Standard proctor test was performed on the soil in consideration and a specimen having a radius of 2.5 inches and height of 2.1 inches was trimmed out from the extract after compaction. Soil samples were prepared at 2%, 4%, 6% dry and wet of optimum and the bender elements were installed in the sample to measure the shear wave velocity. The soil specimen was then placed in a container with water and left for 24 hours allowing it to wet from the bottom along the sides of the specimen. The shear wave velocity was again measured after 48 hours and the soil sample was measured for water content after wetting.

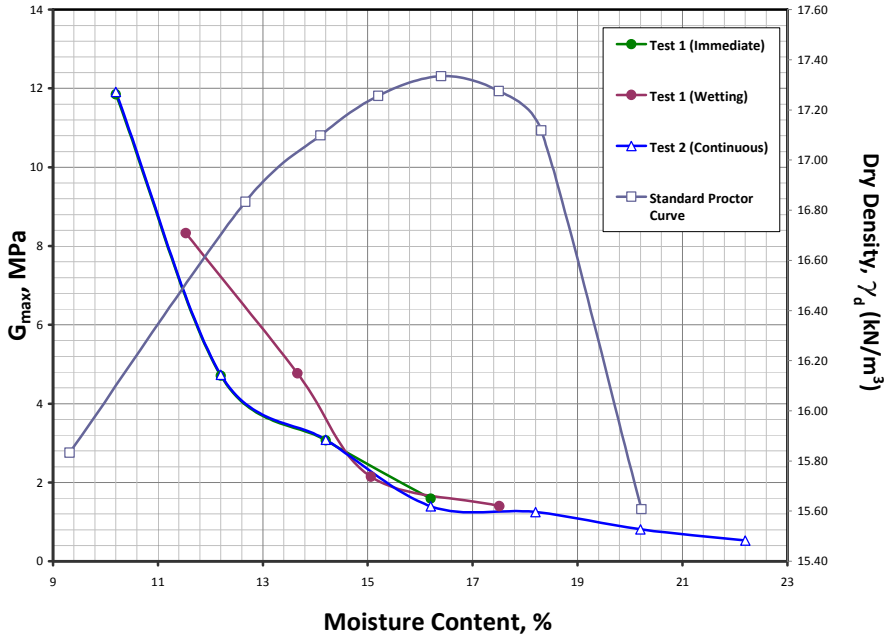

FIG 4.5: Stiffness of the soil along the compaction curve

Two types of tests were performed in this category, one being with four different soil samples prepared at 6%, 4%, 2% dry of optimum and the fourth one prepared at optimum moisture content. These four samples are allowed to wet for 48 hours after taking the shear wave velocity measurements initially, with the error due to evaporation of water being neglected with the room temperature at 25 ± 0.5^{0}C. The stiffness of the soil at these different water contents was

found to decrease with the increase in initial water content and decrease with the wetting water contents as well. The experimental setup of this procedure has been explained clearly in Chapter 3. The variation of the shear stiffness with water content can be seen in Figure 4.5.

In the second type of test, one soil sample was prepared at a moisture content of 6% dry of optimum and the initial shear wave measurements were performed. The sample was then placed in as container of water to be allowed to wet from the bottom and the top of the soil sample was covered with a aluminium foil to prevent evaporation of water and to prevent surface drying. The bender elemnent was installed through a small hole on top of the foil. The change in weight of the specimen was continuously recorded until the weight of the sample reached the desired wetting water content and then a reading was taken to measure the shear wave velocity. It was observed that there is no significant change in the stiffness values when the measurement were performed in this manner and the rate of change of water content was observed to be significanly faster during the course of the experiment spanning 12 days.

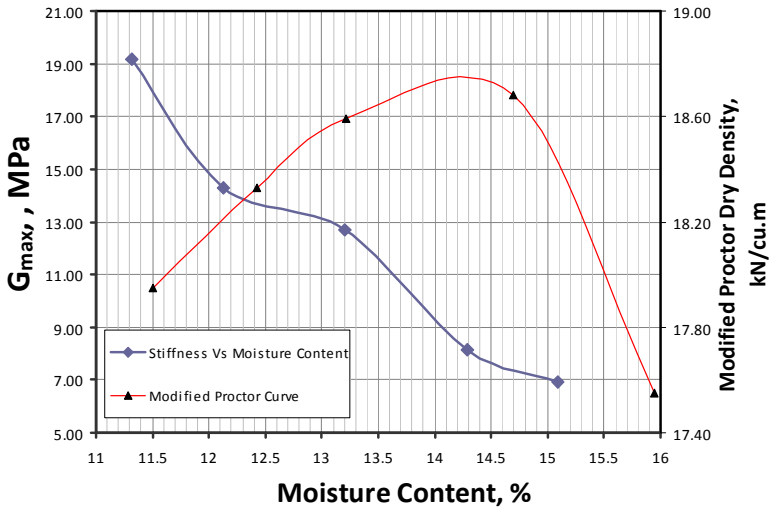

FIG 4.6: Variation of stiffness along continuous wetting for a modified proctor test

The results from the experiment are presented in Figure 4.5 observing the trend to be similar to the results obtained in the previous type of testing. This shows that with increase in

water content, the stiffness of the soil decreases non-linearly. The behavior of the soil along the wetting paths of these two test methods have been similar, with the stiffness values also within 6% of the value determined at that particular water content. Hence, we could conclude that both the methods of determining the stiffness of the soil yield the same result showing that the stiffness of the soil decrease along the standard proctor curve with increase in soil moisture content. Stiffness measurements were made on samples compacted using the modified proctor technique. The measurements followed the same trend of decreasing stiffness with increase in moisture content. The value of stiffness increased due to the increase in the compaction energy on the soil. The results from the experiment is presented in Figure 4.6.

4.5. Experimental Results of Stiffness (G_{max}) along the Consolidation Curve

Standard proctor test were performed on the soil and the specimens were trimmed out from the extract after compaction. Soil samples were prepared at optimum moisture content and allowed to consolidate to pressures of 0, 50, 100, 150, 200, 300, 400 kPa for 48 hours.

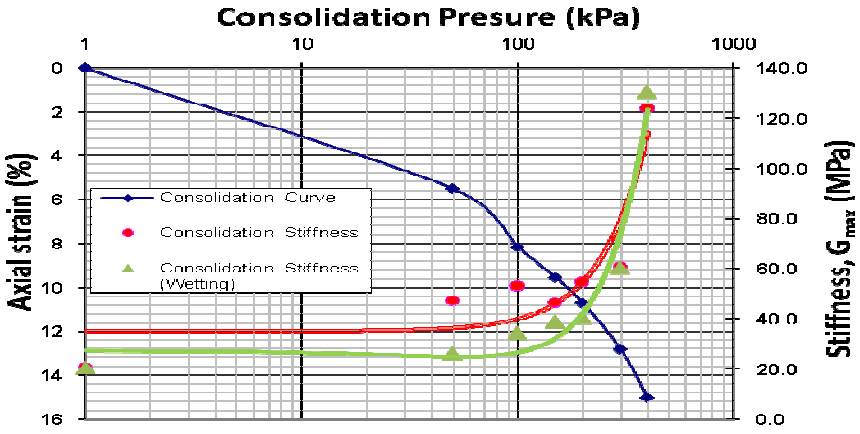

FIG 4.7: Influence of consolidation on stiffness (2.5 inches X 2.1 inches)

The bender elements were then installed in the sample to measure the shear wave velocity. The tests were conducted in a standard consolidation mold of size 2.5 inches diameter and 1.0 inches in height and another test in a specimen of size 2.5 inches diameter and 2.1 inches

in height. The stiffness of the soil in the two specimen sizes was found to increase with increase in the consolidation pressure and decrease with wetting when compared to the stiffness after 48 hours of application of the consolidation pressure. The variation of the shear stiffness with consolidation pressure and water content can be seen in Figure 4.7 and Figure 4.8. The size of the specimen did not affect the stiffness in any way but the stiffness was found to increase appreciably after the pre-consolidation pressure of 96 kPa of the soil was reached. It can be concluded that the stiffness of the soil increases as the consolidation pressure increases.

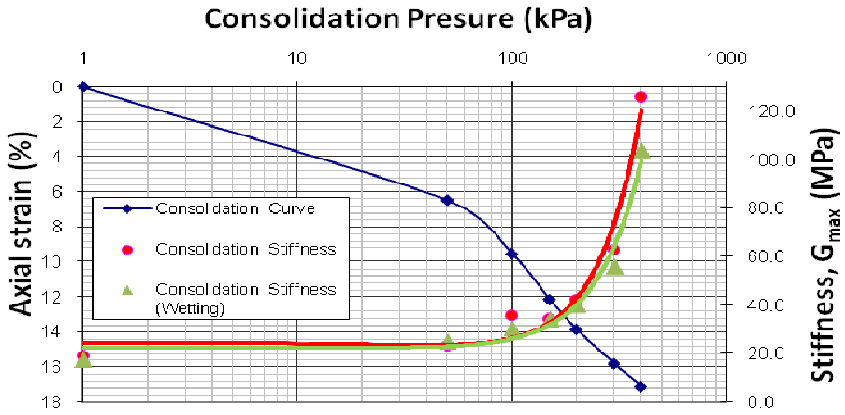

FIG 4.8: Influence of consolidation on stiffness (2.5 inches X 1 inch)

4.6 Experimental Variation of Stiffness (G_{max}) with the Undrained Shear Strength (S_u)

Standard proctor tests were performed on the soil and the specimens were trimmed out from the extract after compaction. The extract from the standard proctor mold was cut into 4 equal parts with a wire gauge and samples of 38 mm (1.5 inches) diameter and 76 mm (3 inches) height were prepared. The samples are in the standard sizes (height to diameter ratio is 2:1) of the triaxial specimen, but to facilitate the generation of shear waves, the height of the sample was reduced to 30mm cut from the middle portion of the sample. Soil samples were prepared at the optimum moisture content and were subjected to cell pressures of 0, 100, 200, 300, 400 kPa at an applied axial strain of 25% which is the loading zone.

TABLE 4.4 (a): Calculation of results from the consolidation test - Test 1

Length	5.25	cm				Density	20.17	kN/m^3			
Moisture Content	Pressure	Time	Velocity	G_{max}	Strain	Moisture Content	Pressure	Time	Velocity	G_{max}	Strain
%	kPa	s	m/s	MPa	%	%	kPa	s	m/s	MPa	%
16.2	1	0.001635	32.110	20.796	0	17.63	1	0.001635	32.110	20.796	0
15.91	50	0.001085	48.387	47.224	5.49	16.87	50	0.001453	36.145	26.351	5.49
15.65	100	0.001023	51.345	53.174	8.15	16.41	100	0.001268	41.420	34.604	8.15
15.42	150	0.001095	47.945	46.366	9.54	15.96	150	0.001193	44.025	39.094	9.54
14.98	200	0.001008	52.109	54.769	10.7	15.63	200	0.00117	44.872	40.612	10.7
14.53	300	0.000958	54.830	60.638	12.81	15.11	300	0.000958	54.830	60.638	12.88
14.21	400	0.00067	78.358	123.844	15.01	14.87	400	0.000653	80.460	130.576	15.01

TABLE 4.4 (b): Test 2

Length	1.94	cm				Density	20.17	kN/m^3			
Moisture Content	Pressure	Time	Velocity	G_{max}	Strain	Moisture Content	Pressure	Time	Velocity	G_{max}	Strain
%	kPa	s	m/s	MPa	%	%	kPa	s	m/s	MPa	%
16.2	1	0.000541	35.871	19.134	0	16.94	1	0.000565	34.3667	17.564	0
15.97	50	0.000491	39.546	23.257	6.48	16.76	50	0.000474	40.90813	24.886	6.48
15.73	100	0.000395	49.064	35.799	9.54	16.31	100	0.00043	45.13377	30.293	9.54
15.48	150	0.000404	48.055	34.342	12.15	16.03	150	0.000405	47.96044	34.206	12.15
15.09	200	0.000364	53.272	42.203	13.86	15.77	200	0.000374	51.91793	40.084	13.86
14.71	300	0.000298	65.028	62.884	15.81	15.23	300	0.000317	61.26316	55.813	15.81
14.32	400	0.000211	92.016	125.911	17.13	14.91	400	0.000232	83.50072	103.685	17.13

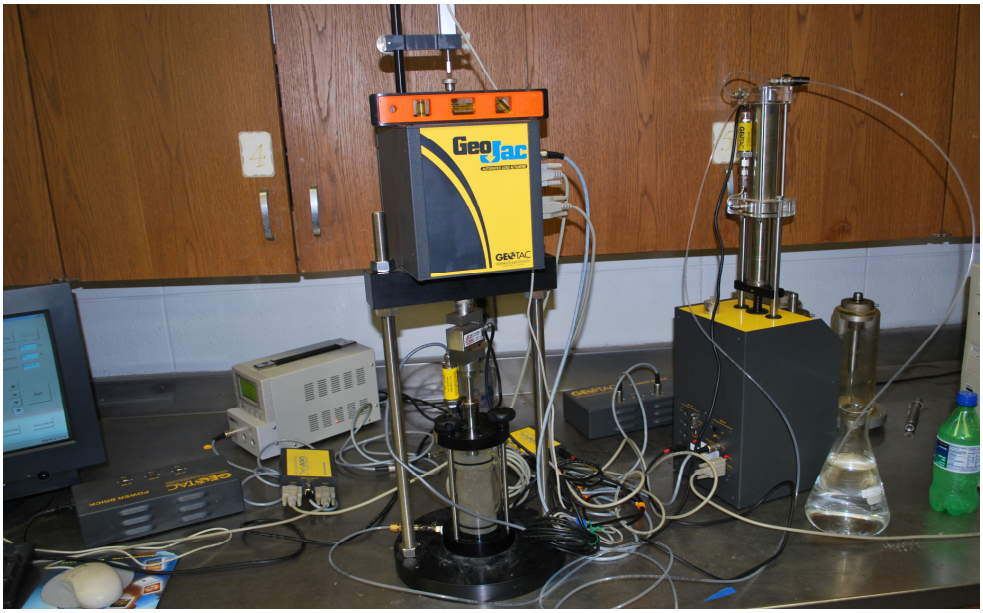

FIG 4.9: A view of the experimental set-up of the sample in the UU test

According to ASTM 2850, if the soil doesn't fail before 15 % axial strain, then the failure stress is considered to be the deviator stress at that strain. The load is applied automatically by the loading machine (GeoJac) due to the axial strain applied. This gives us the variation of deviator stress and the axial strain at the five different isotropic conditions as shown in Figure 4.10. Half of the peak value of the deviator stress for a particular confining pressure is considered as the undrained shear strength (S_u) of the specimen at that confining pressure. The specimen was then removed out of the cell and the membrane was carefully cut without disturbing the sample and to enable the installation of bender elements in the sample to measure the shear wave velocity. The variation of stiffness (G_{max}) with undrained shear strength can be seen in Figure 4.11 and it can be concluded that stiffness decreases with increase in cell pressure whereas the undrained shear strength increases concluding the fact that small strain shear stiffness (G_{max}) and the undrained shear strength are inversely proportional to each other i.e., as stiffness increases, the undrained shear strength decreases and vice versa. The results of the test are shown in Table 4.5.

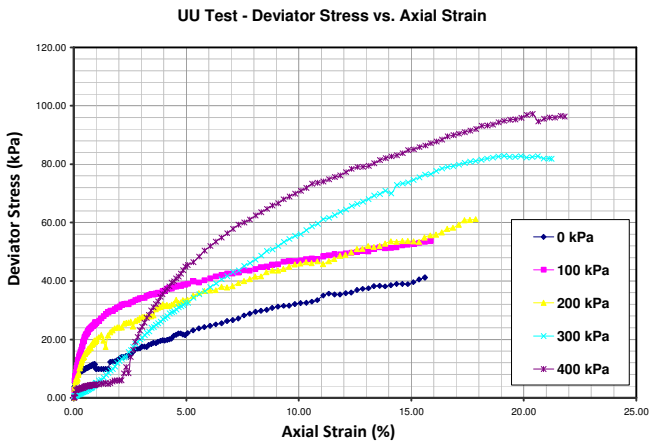

FIG 4.10: Variation of deviator stress and axial strain in the UU test

TABLE 4.5: Calculation of results from the unconsolidated undrained (UU) test

Length	*3.1*	*cm*			
Cell pressure	**Peak Stress**	**Peak Strain**	**Time**	**V_s**	**G_{max}**
kPa	**kPa**	**%**	S	m/s	**kPa**
0	44.33	11.10	0.0064	5.00	494.73
100	46.96	15.00	0.0072	4.44	390.90
200	61.19	17.86	0.0076	4.21	350.83
300	82.82	19.13	0.008	4.00	316.62
400	97.19	20.40	0.009	3.56	250.17

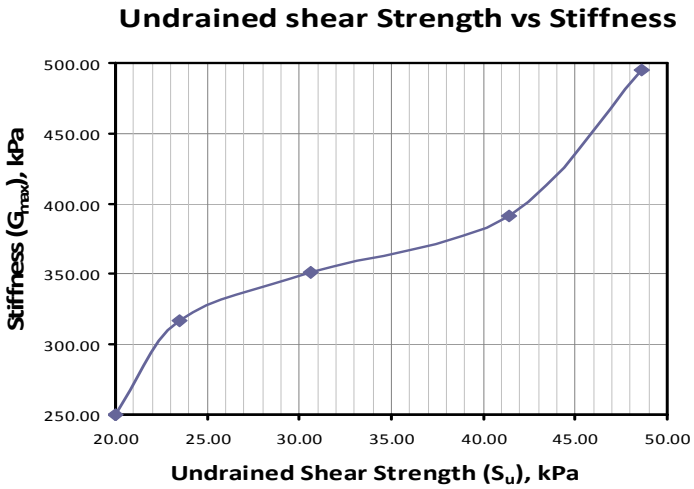

FIG 4.11: Variation of stiffness (G_{max}) with undrained shear strength (S_u)

TABLE 4.6 (a): Calculation of results from the unsaturated triaxial test - Test 1

Specific Gravity	G_s	2.71	
Wt. of dry soil		338.30	g
Volume of Sample	V	196.25	cc
Vol. of dry soil	$V_s=W_s/G_s$	124.83	cc
Vol. of Voids	$V_v=V-V_s$	71.42	cc
Void Ratio	$e=V_v/V_s$	0.57	
Specific Volume	$\nu=1+e$	1.57	
Dry Density	$\rho_{dry}=W_s/V$	1.72	g/cc
Density	$\rho=\rho_{dry}*(1+w)$		
Length between BE		4.00	cm

Suction	Wet soil	Weight of soil after test	Initial Water Content	Final Water Content	Burette Reading	Density	Time	Vs	G_{max}
kPa	g	g	%	%	ml	kNs^2/m^4	s	m/s	MPa
1	407.6	407.4	20.48	20.43	10	20.36	2.33E-03	17.17	6.00
100	407.2	393.7	20.37	16.38	21	19.68	2.20E-03	18.18	6.51
200	406.9	381.3	20.28	12.71	33	19.06	1.74E-03	22.99	10.07
300	407.2	365.8	20.37	8.13	46	18.29	1.45E-03	27.59	13.92
400	407.3	352.1	20.40	4.08	58	17.60	1.42E-03	28.17	13.97
300	407.2	360.4	20.37	6.53	51	18.02	1.44E-03	27.78	13.90
200	407.8	371.2	20.54	9.73	61	18.56	1.67E-03	23.95	10.65
100	407.3	382.8	20.40	13.15	69	19.14	2.11E-03	18.96	6.88

(Table Continued)

TABLE 4.6 (b): Test 2

Specific Gravity	Gs	2.71	
Wt. of dry soil		348.00	g
Volume of Sample	V	196.25	cc
Vol. of dry soil	Vs=Ws/Gs	128.41	cc
Vol. of Voids	Vv=V-Vs	67.84	cc
Void Ratio	e=Vv/Vs	0.53	
Specific Volume	ν=1+e	1.53	
Dry Density	ρ_{dry}=Ws/V	1.77	g/cc
Density	$\rho=\rho_{dry}*(1+w)$		
Length between BE		4.20	cm

Suction	Wet soil	Weight of soil after test	Initial Water Content	Final Water Content	Burette Readings	Density	Time	V_s	G_{max}
kPa	g	g	%	%	ml	kNs^2/m^4	s	m/s	MPa
1	413	413	18.68	18.68	20	20.64	2.30E-03	18.26	6.88
100	413	399	18.68	14.66	32	19.94	1.92E-03	21.88	9.54
200	411	387	18.10	11.21	44	19.35	1.66E-03	25.30	12.38
100	411	394	18.10	13.22	37	19.69	1.88E-03	22.34	9.83

4.7 Experimental Variation of Stiffness (G_{max}) along the Wetting and Drying SWCC

A double walled triaxial test was performed to determine the wetting soil water characteristic curve. The test was performed on a specimen of height 100mm and diameter 50 mm. The procedure has been clearly outlined in Chapter 3 for reference. This test proved the assumption that soil stiffness (G_{max}) has a profound hysteresis with the water content (w%) with the stiffness decreasing along the wetting curve but its value being greater than the value of stiffness along the drying curve at the same value of matric suction (u_a-u_w). Wheeler et al (2001) showed the hysteresis of the soil water characteristic curve and with the help of this study, the hysteresis of soil stiffness also takes limelight. Figure 4.12, Figure 4.13 and Figure 4.14 show the soil water characteristic curve and the variation of stiffness respectively with the tabular calculations shown in Table 4.6.

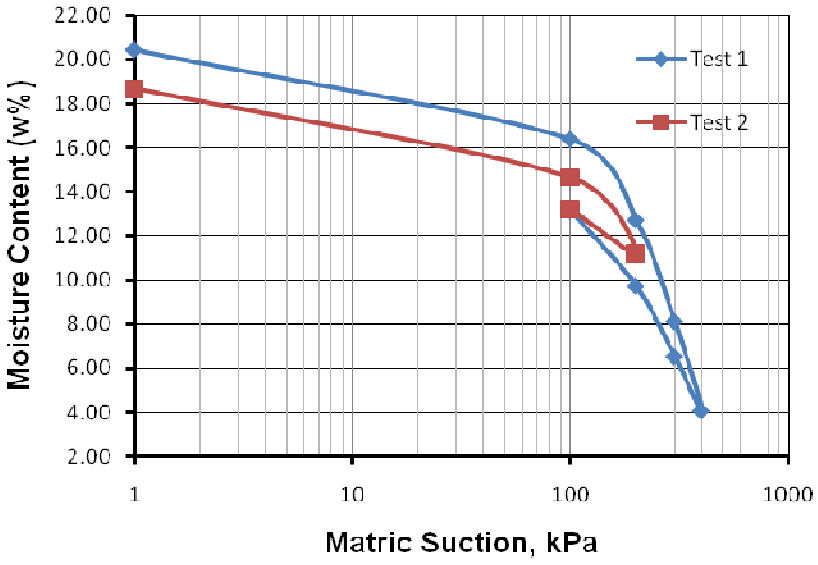

FIG 4.12: Variation of matric suction (u_a-u_w) with moisture content (w %)

The test was performed using the same equilibration time of 24 hours used to determine the SWCC using the Fredlund's device but it was observed that the amount of water coming out of the soil was a bit higher than the previous test. This can be attributed to the fact that in the Fredlund's test, the soil sample was compressed in one dimension but in

the triaxial test, the soil sample was subjected to pressure from all the direction and thus the change in void ratio of the soil is comparatively higher in the latter study. Stiffness of the soil was determined using the same wave propagation technique, but the sample size was reduced to 40mm so as to reduce the errors in the determination of the travel time of the shear wave.

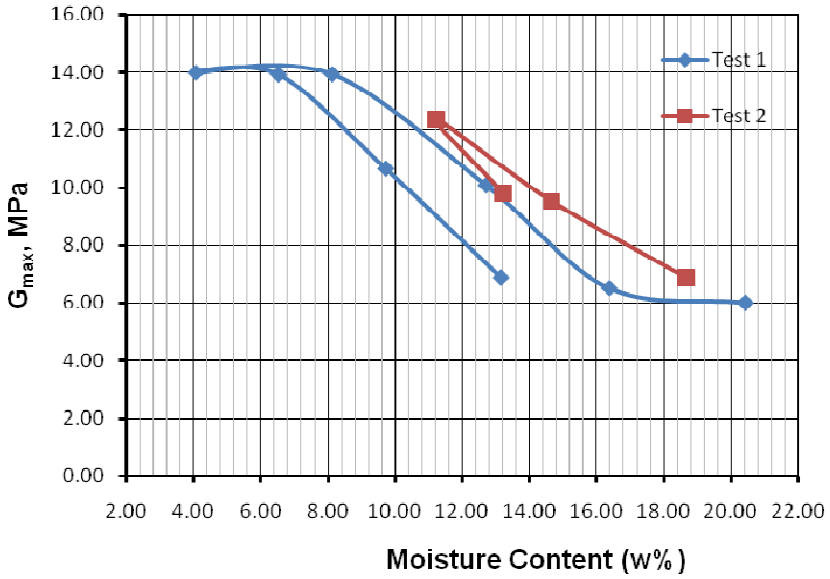

FIG 4.13: Variation of stiffness (G_{max}) with moisture content (w %)

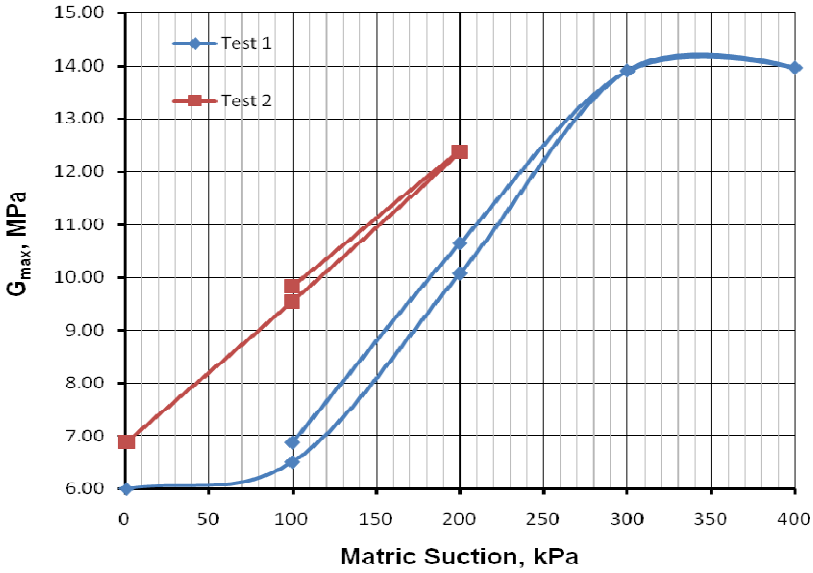

FIG 4.14: Variation of stiffness (G_{max}) against matric suction (u_a-u_w)

CHAPTER 5 STATISTICAL ANALYSIS AND DISCUSSION

5.1 Introduction

In this chapter, the results from the regression analysis performed on the data obtained are presented and the best-fit line is shown. Statistical analysis using the t – distribution was performed assuming 95 % confidence in the data obtained. The model of analysis would be the same for the data obtained with the p-value changing for different data and the type of the regression curve plotted. This analysis was applied only to the soil that was tested.

5.2 Statistical Model for Stiffness (G_{max}) and Moisture Content (w %)

Stiffness and moisture content are plotted against each other to find out the trend along which the stiffness varies with moisture content to be able to compare it with the soil water characteristic curve. Let X denotes the moisture content. For X fixed, Y_x denotes stiffness of the soil selected from the huge area of soil receiving moisture content, X. For the purpose of this study, set the bound on Type – I error with $\alpha = 0.05$

Y_x is N [E (Y_x) = μ (X), σ^2] and all the Y's (Stiffness values) are independent.

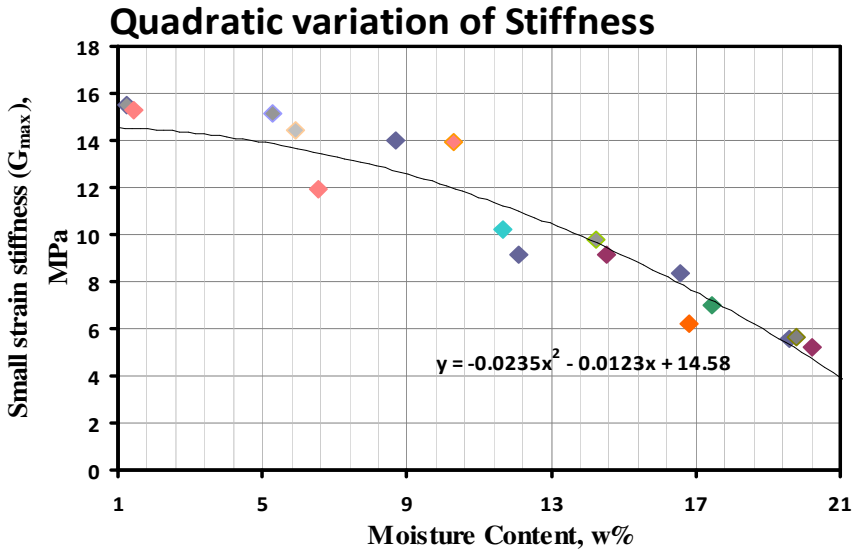

FIG 5.1: Quadratic variation of stiffness (G_{max}) and moisture content (w %)

Now, based on the data available for moisture content and stiffness, testing the regression

analysis by trying to fit a quadratic curve and a cubic curve for the data and the results of each fit is shown in Figure 5.1.

Let $\mu(X) = \beta_0 + \beta_1 X + \beta_2 X^2$ be the equation of the quadratic curve. $E(Y_{x^*}) = \mu(X^*)$ is the population average stiffness for that population of soil with X* moisture content.

The regression model is defined as

Y_{x^*} is N $[E(Y_{x^*}) = \mu(X^*) = \beta_0 + \beta_1 X^* + \beta_2 X^{*2}, \sigma^2]$

To test the model, I performed a Null hypothesis on 'β_2' making it equal to zero and the alternate proving the null to be false.

H_0: $\beta_2 = 0$ and H_A: H_0 is false

From the SAS printout, $\beta_2 = -0.02352$ and $S_{\beta 2} = 0.00891$,

Testing the hypothesis, $\frac{\beta_2 - 0}{S_{\beta 2}} = -2.64$

Performing a t – test, p-value = 0.0186 which is less than 0.05 and hence, the null is rejected and the assumed quadratic regression is a correct least squares fit for the Stiffness-Moisture content relationship.

Similarly, while fitting a cubic curve to the relationship the following results were obtained and shown in Figure 5.2.

$\mu(X) = \beta_0 + \beta_1 X + \beta_2 X^2 + \beta_3 X^3$ be the equation of the cubic curve.

The regression model is defined as

Y_{x^*} is N $[E(Y_{x^*}) = \mu(X^*) = \beta_0 + \beta_1 X^* + \beta_2 X^{*2} + \beta_3 X^{*3}, \sigma^2]$

To test the model, I performed a Null hypothesis on 'β_2' making it equal to zero and the alternate proving the null to be false.

H_0: $\beta_3 = 0$ and H_A: H_0 is false

From the SAS printout, $\beta_3 = 0.00260$ and $S_{\beta 3} = 0.00173$,

Testing the hypothesis, p-value = $\frac{\beta_3 - 0}{S_{\beta 3}} = 1.50$

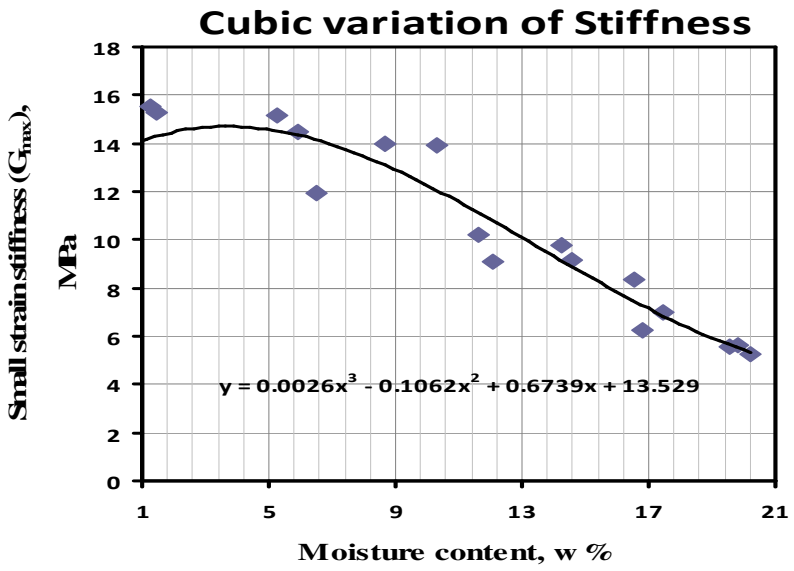

FIG 5.2: Cubic variation of stiffness (G_{max}) and moisture content (w %)

Performing a t – test, p-value = 0.1548 which is greater than 0.05 and hence, the null is accepted and the assumed cubic regression is not a correct least squares fit and hence, a quadratic regression is a correct least squares fit for the Stiffness-Moisture content relationship. The limit of these results are between suction ranges of 0 – 400 kPa and the soil specimen prepared at the optimum moisture content.

5.3 Statistical Model for Stiffness (G_{max}) Vs. Suction

Stiffness and suction are plotted against each other to find out the trend along which the stiffness varies with soil suction. Let X denotes the suction. For X fixed, Y_x denotes stiffness of the soil selected from the huge area of soil receiving suction, X. For the purpose of this study, I'll set the bound on Type – I error with $\alpha = 0.05$.

Y_x is N [E (Y_x) = μ (X), σ^2] and all the Y's (Stiffness values) are independent.

Now, based on the data available for suction and stiffness, I tested the regression analysis by

trying to fit a quadratic curve and a cubic curve for the data and the results of each fit are shown in Figure 5.3 and Figure 5.4 respectively.

Let $\mu(X) = \beta_0 + \beta_1 X + \beta_2 X^2$ be the equation of the quadratic curve.

$E(Y_{x^*}) = \mu(X^*)$ is the population average stiffness for that population of soil with X* suction.

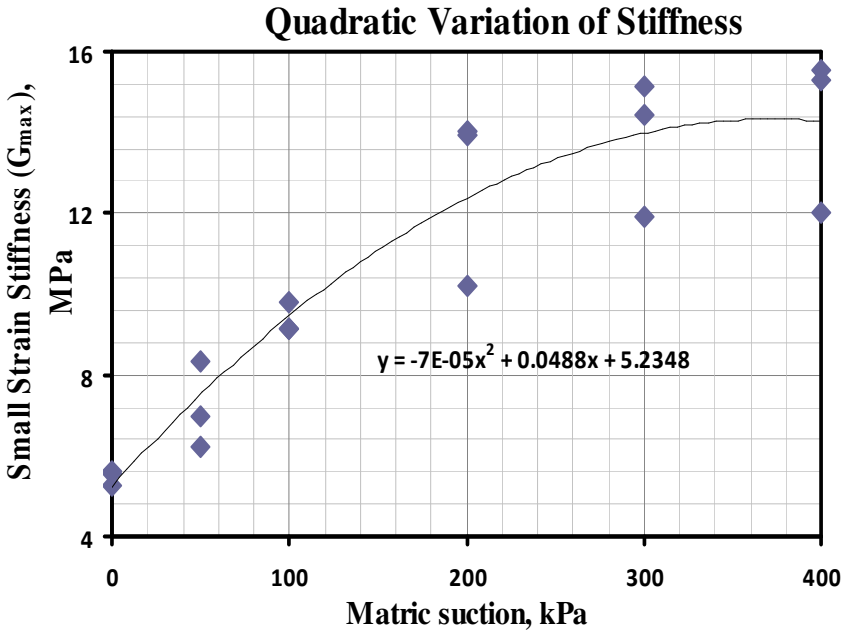

FIG 5.3: Quadratic variation of stiffness (G_{max}) vs. matric suction ($u_a - u_w$)

The regression model is defined as

Y_{x^*} is N $[E(Y_{x^*}) = \mu(X^*) = \beta_0 + \beta_1 X^* + \beta_2 X^{*2}, \sigma^2]$

To test the model, I performed a Null hypothesis on 'β_2' making it equal to zero and the alternate proving the null to be false.

H_0: $\beta_2 = 0$ and $H_{A:}$ H_0 is false

From the SAS printout, $\beta_2 = -0.00006549$ and $S_{\beta 2} = 0.00002039$,

Testing the hypothesis, $\dfrac{\beta_2 - 0}{S_{\beta 2}} = -3.21$

Performing a t – test, p-value = 0.0058 which is less than 0.05 and hence, the null is rejected and

the assumed quadratic regression is a correct least squares fit for the Stiffness-Suction relationship.

Similarly, I tried fitting a cubic curve to the relationship and the following results were obtained:

$\mu(X) = \beta_0 + \beta_1 X + \beta_2 X^2 + \beta_3 X^3$ be the equation of the cubic curve.

The regression model is defined as

Y_{x^*} is N $[E(Y_{x^*}) = \mu(X^*) = \beta_0 + \beta_1 X^* + \beta_2 X^{*2} + \beta_3 X^{*3}, \sigma^2]$

To test the model, I performed a Null hypothesis on 'β_2' making it equal to zero and the alternate proving the null to be false.

H_0: $\beta_3 = 0$ and H_A: H_0 is false

From the SAS printout, $\beta_3 = -4.57509E\text{-}8$ and $S_{\beta 3} = 1.94455E\text{-}7$,

Testing the hypothesis, $\dfrac{\beta_3 - 0}{S_{\beta 3}} = -0.24$

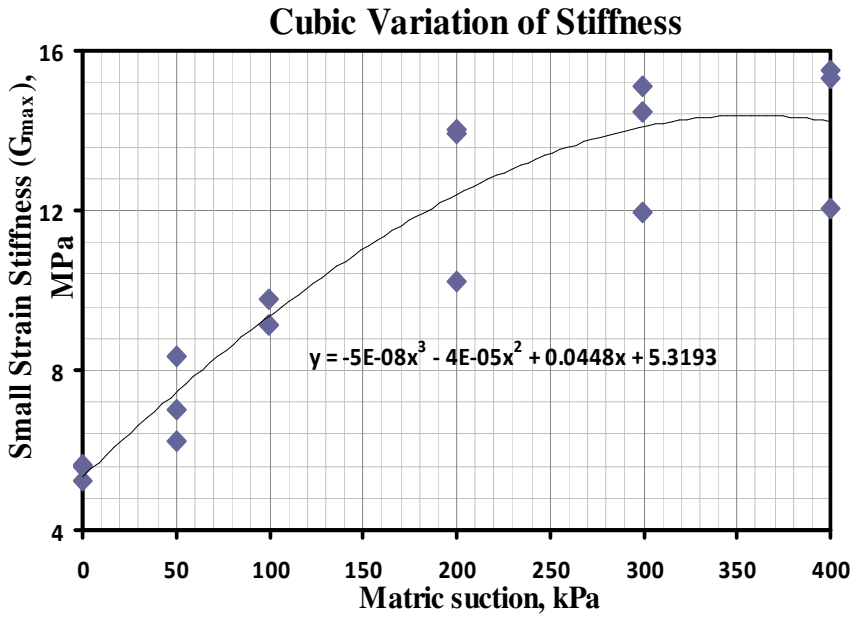

FIG 5.4: Cubic variation of stiffness (G_{max}) vs. matric suction ($u_a - u_w$)

Performing a t – test, p-value = 0.8174 which is greater than 0.05 and hence, the null is accepted and the assumed cubic regression is not a correct least squares fit and hence, a quadratic

regression is a correct least squares fit for the Stiffness-Suction relationship. The limit of these results are between suction ranges of 0 – 400 kPa and the soil specimen prepared at the optimum moisture content.

5.4 Analysis of Results from the Compaction Test

Stiffness and moisture content are plotted against each other to find out the trend along which the stiffness varies with soil moisture content to be able to compare it with the standard proctor curve.

Let X denotes the moisture. For X fixed, Y_x denotes stiffness of the soil selected from the huge area of soil receiving moisture, X. For the purpose of this study, I'll set the bound on Type – I error with $\alpha = 0.05$.

Y_x is N [E (Y_x) = μ (X), σ^2] and all the Y's (Stiffness values) are independent. Now, based on the data available for moisture content and stiffness, I tested the regression analysis by trying to fit a exponential curve for the data and the results of each fit is shown in Figure 5.5.

Let μ (X) = A*e $^{\beta 0x}$ be the equation of the exponential curve. E (Y_{x*}) = μ (X*) is the population average stiffness for that population of soil with X* moisture content.

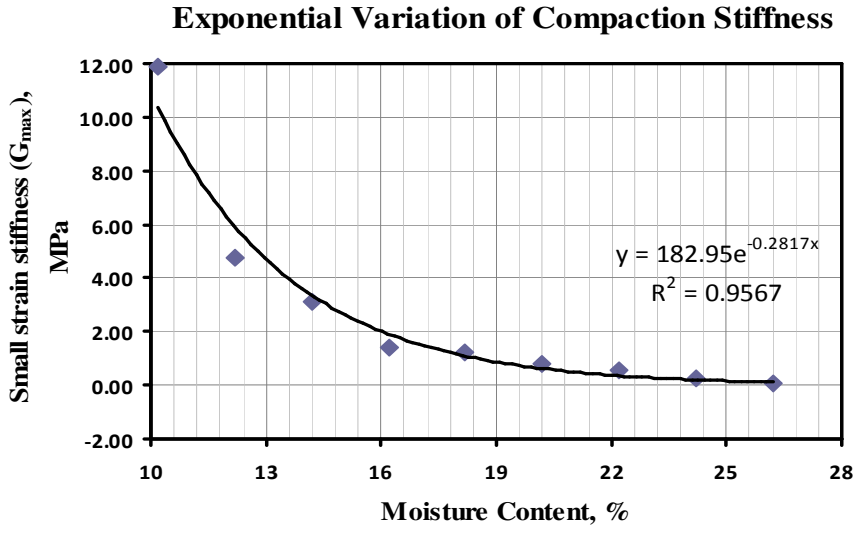

FIG 5.5: Exponential variation of compaction stiffness, G_{max} vs. moisture content

The regression model is defined as

Y_{x^*} is N [E (Y_{x^*}) = μ (X*) = A*e $^{\beta 0x}$, σ^2]

Testing the hypothesis,

Performing a regression, R^2= 0.9567, mean of 2.67 and standard deviation of 3.78. Hence, the exponential curve was the best fit line for the compaction stiffness data.

5.5 Analysis of Results from the Consolidation Test

Consolidation stiffness and consolidation pressure are plotted against each other to find out the trend along which the stiffness varies with the consolidation pressure to be able to compare it with the consolidation curve.

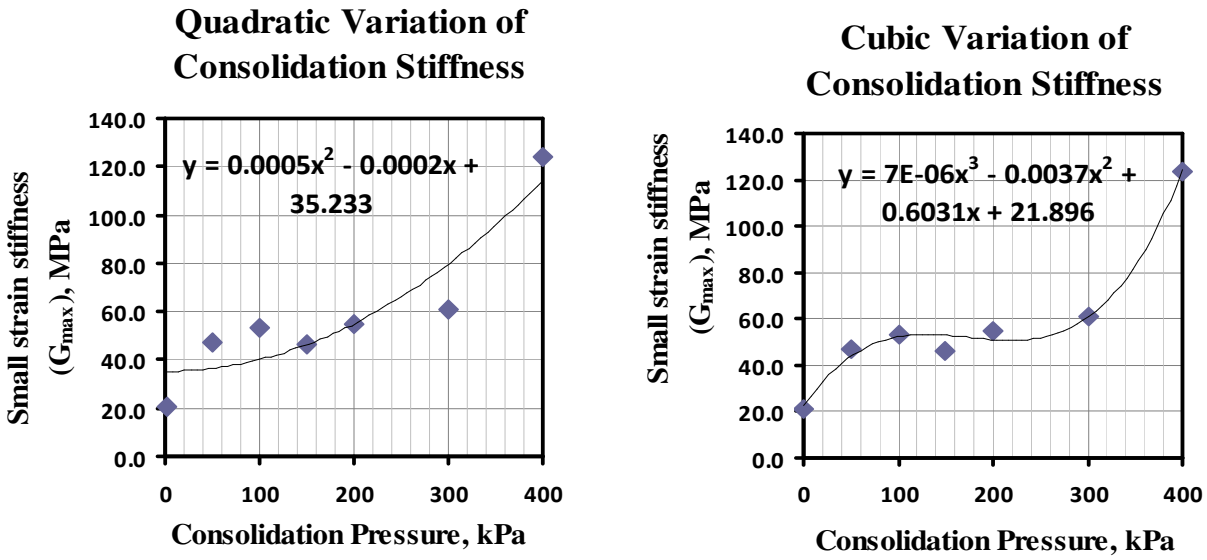

FIG 5.6: Variation consolidation stiffness, G_{max} vs. consolidation pressure

A quadratic and a cubic regression line were plotted similar to the model shown in section 5.2 and the p-values were calculated based on a 95% confidence interval. The fit was considered satisfactory if the p-value was less than 0.05 which is the limit of the Type-1 bound error. Quadratic regression showed that the p-value = 0.2611 which is greater than 0.05 and hence, the assumed quadratic regression is not the correct least squares fit for the consolidation stiffness –

consolidation pressure relationship. Similarly, while fitting a cubic curve the p-value = 0.0093 which is less than 0.05 and hence, the null is rejected and the assumed cubic regression is the correct least squares fit for the Consolidation stiffness – Consolidation pressure relationship. The results of the analysis are shown in Figure 5.6. The limit of these results are between suction ranges of 0 – 400 kPa and the soil specimen prepared at the optimum moisture content.

5.6 Analysis of the Results from the Unconsolidated Undrained (UU) Test

Stiffness and undrained shear strength are plotted against each other to find out the trend along which the stiffness varies with the soil undrained shear strength (S_u). Based on the data available for undrained shear strength and stiffness, we tested the regression analysis by trying to fit a quadratic curve and a cubic curve for the data and the results of each fit are shown in Figure 5.7.

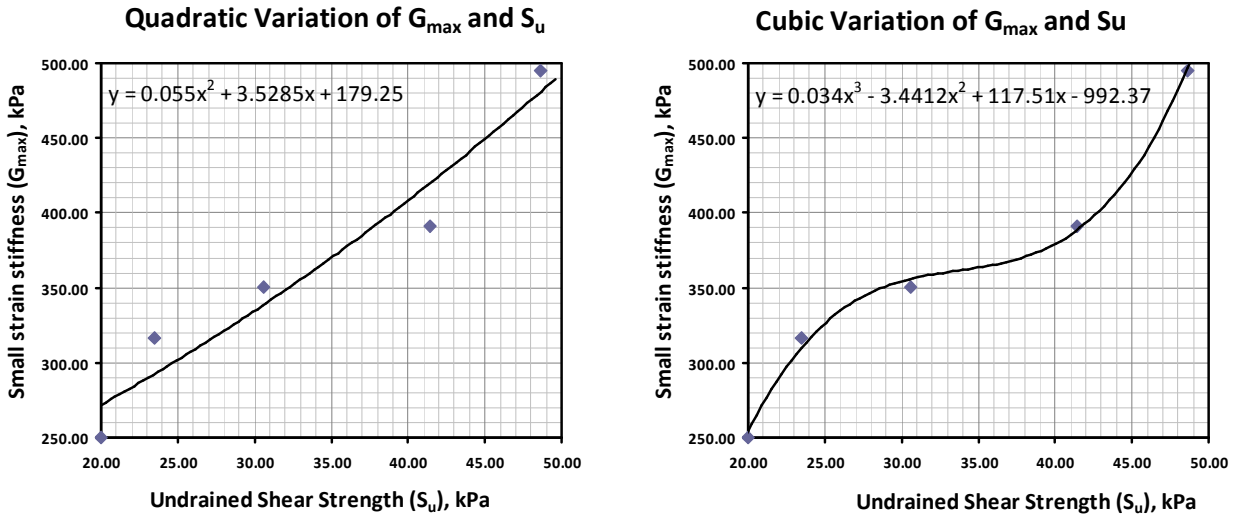

FIG 5.7: Variation of stiffness (G_{max}) vs. undrained shear strength (S_u)

Quadaratic regression gave a p-value = 0.0624 which is greater than 0.05 and hence, the null is accepted and the assumed quadratic regression is not the correct least squares fit for the stiffness – undrained shear strength relationship. Similarly, while fitting a cubic curve to the relationship the p-value = 0.0 which is less than 0.05 and hence, the null is rejected and the assumed cubic regression is the correct least squares fit for the Stiffness – Undrained shear

strength relationship. Regression analysis could not be performed on the results received from the unsaturated triaxial device due to the presence of the wetting curve on the same chart but it may be concluded that the variation of the wetting curve would be similar to a drying curve which would be a quadratic variation.

CHAPTER 6 CONCLUSIONS AND RECOMMENDATIONS

6.1 Introduction

This chapter presents the summary of the main features of the research, major conclusions of the study and recommendations for future work. The research focused on investigating soil stiffness and its correlation with the wetting drying cycles of the soil. Influences of moisture content, consolidation pressure and undrained shear strength on the stiffness of low plasticity silty clay (CL) are presented.

6.2 Conclusions

The behavior of small strain stiffness of the soil along the wetting drying paths was to be predicted at different levels of soil matric suction (u_a - u_w) and the pore water pressure (u_w = 0) was zero as it was open to atmosphere. The tests were conducted in two different kinds of test setup. The first objective of this study was to determine the drying curve of the soil. A 1-D soil water characteristic curve device was used for this purpose capable of applying suction to a range of 400kPa. It was observed that the water content of the soil decreases with increase in soil matric suction. As the soil is subjected to higher values of matric suction, the volume of the voids is reduced showing an increase in the stiffness. Stiffness (G_{max}) increased with soil matric suction but in a non-linear fashion as presented by Atkinson, 2000. The trendline was also similar to the one developed by Mancuso et al. (2000) on silty sand shown in Figure 2.6. It could also be concluded that the stiffness increases appreciably once the air – entry value of the soil is reached which was found to be close to 80 kPa. Stiffness of the soil decreases with increase in water content of the soil.

The second objective of this research study was to predict any hysteresis in the stiffness behavior of the soil along the wetting drying paths similar to the hysteresis of the soil water characteristic curve predicted by Wheeler et al. (2003). To conduct this study, an unsaturated

triaxial cell was adopted with the end platens installed with low air entry as well as high air entry filters. It was observed that the stiffness of the soil increases with increase in matric suction along the drying side and decreases with decrease in matric suction along the wetting side but, to a value higher than the value obtained at that matric suction along the drying curve. This shows that there is a significant hysteresis in the mechanical behavior of soil stiffness along the wetting and drying parts of the soil.

The third objective of this study was to determine the variation of stiffness along the standard proctor curve, the consolidation curve and against the undrained shear strength (S_u). It was observed that stiffness (G_{max}) decreases with increase in moisture content of the soil both along the dry and wet sides of the optimum moisture content, in the case of a standard proctor sample as well as a modified proctor sample. The values of stiffness of the modified proctor sample is greater than that of the standard proctor sample and this can be attributed to the fact that increase in compaction energy reduces the soil voids and hence increases the stiffness of the soil.

The stiffness (G_{max}) of the soil increases with increase in consolidation pressure but increases appreciably once the pre-consolidation pressure of 96 kPa for the soil is reached and also the stiffness (G_{max}) increases with an increase in the undrained shear strength (S_u) of the soil. The fourth objective of this study was to analyze the variation of stiffness with matric suction using regression analysis. SAS program was used to do this analysis and it was concluded that stiffness (G_{max}) of the soil varies quadratically with soil matric suction (u_a - u_w). Stiffness varies exponentially with increase in water content for compacted soil samples. Also, it was concluded that a cubic or a third degree variation is found between stiffness (G_{max}) and the consolidation pressure of the soil as well as the undrained shear strength (S_u) of the soil. SAS program gives out the p - values and to check the results, a Type – I error with 95% confidence interval was

assumed.

6.3 Recommendations

- The research study was conducted assuming that the pore – water pressure (u_w) is zero. In unsaturated soils, pore water pressure is generally not zero and hence, this phenomenon can be a major step in the extension of this research study.
- Tests can be performed on different soil types with different plasticity indexes compared.
- In-situ field stiffness measurements can be performed on the same soil to back calculate the results and compare the results obtained in the field and the laboratory as proposed by Atkinson (2000).
- The research study was done assuming the soil is isotropic which is not ideally the case and hence, this study can be extended to the anisotropic behavior of the soils
- Use of a high air entry value ceramic stone with greater capacity in the GCTS cell could extend the drying soil water characteristic curve which has been found to have a cubic or a 3rd degree variation with degree of saturation and can be extended to determine the stiffness variation which can be assumed to be cubic in such a case.
- The size of the ceramic stone in the GCTS cell can be reduced so as to determine the wetting curve from the cell itself. Incorporation of bender elements over the ceramic stone itself would be a great boon for measuring small strain stiffness against matric suction.
- Finally, the use of electronic and digital equipments for controlling air and water pressure can be used to minimize parallax and other errors in measurement.

REFERENCES

Aitchison, G. D. (1973). “The quantitative description of the stress deformation behavior of expansive soils.” Proceedings of the 3rd International Conference on Expansive Soils, Haifa, Israel, Vol. 2, pp. 79–82.

Aitchison, G. D. (1965). “Soil properties, shear strength, and consolidation.” Proceedings of the 6th International Conference on Soil Mechanics and Foundation and Engineering, Montreal, Canada, Vol. 3, pp. 318–321.

Aitchison, G.D. (1961). “Relationships of moisture stress and effective stress functions in unsaturated soils.” Conference on Pore Pressure and Suction in Soils, London, pp. 47-52.

Arulnathan, R., Boulanger, R.W. and Reimer, M.F. (1998). “Analysis of bender element tests.” Geotechnical Testing Journal, Vol. 21, No. 2, pp. 120-131.

Atkinson, J.H. (2000). “Non-linear soil stiffness in routine design.” Geotechnique, Vol. 50, No. 5, pp. 487-508.

Atkinson, J. H., Sallfors, G. (1991). “Experimental investigation of Stress-Strain-Time characteristics for Laboratory and In-situ tests.” Deformation of soils and displacement of structures (Proc X ECSMFE) AA Balkema, Rotterdam, No. 3, pp. 915-956.

Alramahi, B., Alshibli, K.A., Fratta, D., Trautwein, S. (2008). “A Suction-Control Apparatus for the Measurement of P and S-wave Velocity in Soils.” Geotechnical testing Journal, Vol. 31 (1),

Alramahi, B. (2007). “Characterization of unsaturated soils using elastic and electromagnetic waves.” PhD thesis, Louisiana state university, pp. 01-151.

Blatz, J.A., Graham, J. and Chandler, N.A. (2002). “Influence of suction on the strength and stiffness of compacted sand-bentonite.” Canadian Geotechnical Journal, Vol. 39, pp. 1005-1015.

Bishop, A.W. (1959). “The principle of effective stress.” Teknisk Ukeblad, Vol. 39, pp. 859-863.

Bishop A.W. and Wesley L.D. (1975). “A hydraulic apparatus for controlled stress path testing.” Geotechnique, Vol. 25, No. 4, pp. 657-670.

Bishop A.W. and Blight, G.E. (1963). “Some aspects of effective stress in saturated and unsaturated soils.” Geotechnique, Vol. 13, pp. 177–197.

Bishop, A.W., and Eldin, A.K.G. (1950). "Undrained triaxial tests on saturated sands and their significance in the general theory of shear strength," Geotechnique, Vol. 2, No. 1, pp.

Brand, E.W. (1981). “Some thoughts on rain-induced slope failures.” Proceedings of the 10th International Conference on Soil Mechanics and Foundation Engineering, Vol. 3, Balkema,

Rotterdam, Netherlands, pp. 377–384.

Burland, J.B. and Georgiannou, V.N. (1991). "Small strain stiffness under generalized stress changes." Proceedings of the International Conference on Soil Mechanics and Foundation Engineering, Vol.1, Deformation of Soils and Displacements of Structures X ECSMFE, pp. 41-44.

Cabarkapa, Z., Cuccovillo, T. (2005). "Automated triaxial apparatus for testing unsaturated soils." Geotechnical Testing Journal, Vol. 29, No. 1, pp. 21-29.

Cabarkapa Z., Cuccovillo T., Gunn M. (1999). "Some aspects of the pre-failure behavior of unsaturated soil." Proceedings of II International Conference on pre-failure behavior of geomaterials, Vol. 1, pp. 159-165.

Claudia Festa, Angel Palomino, Tae Sup Yun, Jong Sub Lee. (2001). "Simple procedure for Assembly of Bender Elements." PP presentation, Particulate Media Research Laboratory, Georgia Institute of Technology.

Clayton, C. R. & Heymann, G. (2001). "Stiffness of geomaterials at very small strain." Geotechnique, Vol. 51, No. 5, pp 245 – 255.

Clayton, C.R.I., Theron, M. and Best, A.I. (2004). "The measurement of vertical shear-wave velocity using side-mounted bender elements in the triaxial apparatus." Geotechnique, Vol. 54, No. 7, pp. 495-498.

Croney, D., Coleman, J.D., and Black, W. P. M. (1958). "Movement and distribution of in soil in relation to highway design and performance." Highway Research Board Special Report 40, Water and its Conduction in Soils, National Academy of Science and National Research Council, Washington D. C., pp. 226-252.

Dyvik, R. & Madshus, C. (1985). "Laboratory measurements of G_{max} using bender elements." Proc ASCE Annual Convention: Advances in the Art of Testing Soils under Cyclic Conditions", pp. 186-196.

Eduardo Bilotta., Vito Foresta., & Giancarlo Migliaro. (2006). "Suction controlled laboratory tests on undisturbed pyroclastic soil: stiffness and volumetric deformations." Geotechnical Special Publication No. 147, Unsaturated soils, Vol. 1, pp 849 – 860.

Escario, V. and Juca, F. (1989). "Strength and deformation of partly saturated soils." Proceedings of the 12th International Conference in Soil mechanics and Foundation Engineering, Rio, Balkema, Rotterdam, Vol. 1, pp. 43-46.

Escario, V. and Saez, J. (1986). "The shear strength of partly saturated soils." Géotechnique, Vol. 36, pp. 453-456.

Fam, M.A., Santamarina, J.C. (1995). "Study of geoprocesses with complimentary wave measurements in an oedometer." Geotechnical Testing Journal; Vol. 19, No. 4, pp. 307-314.

Ferber, V., Auriol, J.C., Cui, Y.J., and Magnan, J. P. (2008). "Wetting-induced volume changes in compacted silty clays and high-plasticity clays".Canadian Geotechnical Journal, Vol: 45(2), pp. 252 – 265.

Fiorovante, V. and Capoferri, R. (2001). "On the Use of Multidirectional Piezoelectric Transducers in Triaxial Testing". Geotechnical Testing Journal. Vol. 24. No. 3. pp. 253-255.

Fleureau, J. M., Saoud, K.S., Soemitro, R. and Taibi, S. (1993). "Behavior of clayey soils on drying-wetting paths." Canadian Geotechnical Journal, Vol. 30, pp. 287-296.

Fleureau, J. M., Hadiwardoyo, S. & Gomes Correia, A. (2003). "Generalized effective stress analysis of strength and small strains behavior of a silty sand, from dry to saturated state." Soils and Foundations. Vol. 43, No. 4, pp. 21 – 33.

Fratta, D., Fernandez, A. L., and Santamarina, J. C. (2001). "Geo-Materials: Non-destructive evaluation in Geo-systems." CP 557, Review of Progress in Quantitative Non-destructive Evaluation, Vol. 20, edited by D. O. Thompson and D. E. Chimenti.

Fredlund D.G., Xing A., Fredlund M.D. & Barbour S.L. (1995). "The relationship of the unsaturated soil shear strength to the soil-water characteristic curve." Canadian Geotechnical Journal, Vol. 33, pp. 440-448.

Fredlund, D.J. and Rahardjo, H. (1993). "Soil mechanics for unsaturated soils." John Wiley and Sons, New York, USA, pp. 01-517.

Fredlund, D. G., Morgenstern, N. R., and Widger, R. A. (1978). "The shear strength of unsaturated soil." Canadian Geotechnical Journal, Vol. **15**, pp. 313–321.

Fredlund D.G. and Morgenstern N.R. (1977). "Stress state variables for unsaturated soils." ASCE Journal for Geotechnical Engineering, Divison GT5, Vol. 103, pp. 447-466.

Fung, Y.C. (1977). A First Course in Continuum Mechanics, 2nd edition. Prentice-Hall: Englewood Cliffs, New Jersey, USA, pp.

Gallipoli, D., Gens, A., Sharma, R. and Vaunat, J. (2003). "An elasto-plastic model for unsaturated soil incorporating the effects of suction and degree of saturation on mechanical behavior." Geotechnique, Vol. 53, No. 1, pp. 123-135.

Gan J.K.M., Fredlund D.G and Rahardjo H. (1988). "Determination of the shear strength parameters of an unsaturated soil using the direct shear test." Canadian Geotechnical Journal, Vol. 25, No. 3, pp. 500-510.

Geiser, F., Laloui, L. and Vulliet, L. (2006). "Elasto-plasticity of unsaturated soils: laboratory test results on remolded silt." Soils and Foundations, Vol. 46, No. 5, pp. 545-556.

Georgiannou, V. N., Rampello, S. & Silvestri, F. (1991). "Static and dynamic measurement of

undrained stiffness of natural overconsolidated clay." Proceeding of the X ECSMFE, Florence. Vol. 1, pp 91 - 96.

Gordon, M.A., Clayton, C.R.I. (1997). "Measurement of stiffness of soils using small strain triaxial testing and bender elements." Engineering Geology Special Publication, Vol. 12, pp. 365-371.

Greening, Paul D., Nash, David F.T. (2004). "Frequency domain measurements of G_0 using bender elements." Geotechnical Testing Journal, Vol. 27, No. 3, pp. 288-294.

Hardin, B.O., Blandford, G.E., (1989). "Elasticity of particulate materials." Journal of Geotechnical Engineering, ASCE, Vol. 115, No. 6, pp.788-805.

Hardin, B. O. & Drnevich, V. P. (1972). "Shear modulus and damping in soils: design equations and curves." Journal of Soil Mechanics And Foundation Engineering, ASCE, Vol. 98(SM7), pp. 667 – 682.

Hardin, B. O. and Black, W. L. (1968). "Vibration modulus of normally consolidated clay." Journal of the Soil Mechanic and Foundations Division, ASCE, Vol. 94, pp. 353–368.

Hardin, B.O. and F.E. Richart. (1963). "Elastic wave velocities in granular soils." Journal of the Geotechnical Engineering Division, ASCE, Vol. 89, No. 1, pp. 33-65.

Ishibashi I. and Zhang X. J. (1993). "Unified dynamic shear moduli and damping ratios of sands and clay." Soils Foundations, Vol. 33, No. 1, pp. 182-191.

Jardine, R. J., Symes, M. J. & Burland, J. B. (1984). "The measurement of soil stiffness in the triaxial apparatus." Geotechnique, Vol. 34, No. 3, pp. 323 – 340.

Jennings, J.E. (1961). "A revised effective stress law for use in the prediction of the behavior of unsaturated soils," Conference on Pore Pressure and Suction in Soils, London, pp. 26-30.

Jong Sub Lee and Carlos Santamarina, J. (2005). "Bender elements: performance and signal interpretation." Journal of geotechnical and geoenvironmental engineering. Vol. 131, No 9, pp 1063 – 1070.

Jovicic, V. and Coop, M.R. (1995). "Interpretation of bender element test." Geotechnique, Vol. 45, No. 3, pp. 873-877.

Jovicic, V., Coop, M.R. and Simic, M. (1996). "Objective criteria for determining G_{max} from bender element tests." Geotechnique, Vol. 46, No. 2, pp. 357-362.

Kawaguchi, T., Mitachi, T. and Shibuya, S. 2001. Evaluation of shear wave travel time in laboratory bender element test. Proc. of 15th International Conference on Soil Mechanics and Geotechnical Engineering, Turkey, pp. 155-158.

Kung, T.C., Hsieh C.Y. (2004). "Measurement of shear modulus of soil using bender elements." Journal of Geotechnical and Geo-environmental Engineering, Vol. 35, No. 1, pp. 1-7.

Lambe, T.W., and Whitman, R.V. (1969). *Soil Mechanics*. John Wiley & Sons, New York, USA, pp. 01-553.

Lee, Jong-Sub., Santamarina, J. Carlos. (2005). "Bender elements: performance and signal interpretation." Journal of Geotechnical and Geo-environmental Engineering, Vol. 131, No: 9, pp. 1063-1070.

Leong, E.C., Yeo, S.H. and Rahardjo. (2005). "Measuring shear wave velocity using bender elements." Geotechnical Testing Journal, Vol. 28, No. 5, pp. 488-498.

Leong, E. C., Cahyadi, J., and Rahardjo, H. (2006). "Stiffness of a compacted residual soil." Geotechnical Special Publication No. 147, Unsaturated soils, Vol. 1, pp 1169 – 1180.

Lloret, A. and Alonso, E. E. (1980). "Consolidation of unsaturated soils including swelling and collapse behavior." Geotechnique, Vol. 30, No. 4, pp. 449-447.

Macari E.J. & Hoyos L.R. (2001). "Mechanical behavior of unsaturated soil under multi-axial stress states." Geotechnical Testing Journal, Vol. 24, No. 1, pp. 14-22.

Matyas E.L. and Radhakrishna H.S. (1968). "Volume change characteristics of partially saturated soil." Geotechnique, Vol. 18, pp. 432-448.

Matthews, M. C., Clayton, C. R. I. and Own, Y. (2000). "The use of field geophysical techniques to determine geophysical stiffness parameters." Journal of Geotechnical and Geo-environmental Engineering, Vol. 143, pp. 31-42.

Mancuso, C., Vassallo, R., and d'Onofrio, A. (2002). "Small strain behavior of silty sand in controlled – suction resonant column – torsional shear tests." Canadian Geotechnical Journal, Vol. 39, pp 22 -31.

Marinho, F., Chandler, R., and Crilly, M. (1995). "Stiffness measurement on an unsaturated high plasticity clay using bender elements." Proc. of the 1st International conference on Unsaturated soils. Vol. 2, pp 535 – 539.

Mendoza, C. E, Colmenares, J. E. & Merchan, V. E. (2005). "Stiffness of an unsaturated compacted clayed soil at very small strains." Proc. International Symposium on Advanced Experimental Unsaturated Soil Mechanics, Italy, pp. 199 – 204.

Mendoza, C. E & Colmenares, J. E. (2006). "Influence of the Suction on the stiffness at very small strains." Geotechnical Special Publication No.147, Unsaturated soils, Vol. 1, pp 529 - 540.

Ng, Yung. (2008). "Determination of the anisotropic shear stiffness of an unsaturated decomposed soil", Vol. 58 (1), pp. 23 – 35.

Pennington, Derek S., Nash, David F.T. and Lings, Martin L. (2001). "Horizontally mounted bender elements for measuring anisotropic shear moduli in triaxial clay specimens."

Geotechnical Testing Journal, Vol. 24, No. 2, pp. 133-144.

Perera, Y.Y., Zapata, Z. E., Houston, W. N., Houston, S. L. (2005). "Prediction of the soil water characteristic curve based on grain size distribution and index properties." Proceedings of Geo-Frontiers, Austin, Texas, USA.

Pham, H. Q., Fredlund, D. G. (2008). "Equations for the entire soil-water characteristic curve for a volume change soil." Canadian Geotechnical Journal, Vol. 45 (4), pp. 443 – 453.

Qian, X., Gray, D., & Woods, R. (1993). "Modulus of unsaturated sands." Journal of Geotechnical Engineering, Vol. 119, No. 2, pp 241 – 314.

Qiming, Chen (2007). "An Experimental Study on Characteristics and Behavior of Reinforced Soil Foundation." PhD Thesis, Louisiana State University, pp 01 – 367.

Richards, L. A. (1966). "A soil salinity sensor for improved design." Soil Science Society of America Journal, Vol. 33, pp. 333-337.

Ridley, A.M., Burland, J.B. (1993). "A new instrument to measure soil moisture suction." Geotechnique, Vol. 43, No. 2, pp. 321-324.

Santamarina, J. C., Klein, K. A., and Fam, M. A. (2001). "Soils and Waves." John Wiley and Sons, New York, USA, pp. 1-448.

Sauer, E. K., and Monismith, C. L. (1968). "Influence of soil suction on behavior of a glacial till subjected to repeated loading". Highway Research Record, No. 215, pp 8 – 23.

Sawangsuriya, A., Edil, T. B., and Bosscher, P. J. (2008). "Modulus–suction–moisture relationship for compacted soils**.**" Canadian Geotechnical Journal, Vol. 45 (7), pp. 973 – 983.

Sharma, R. S. (1998). "Mechanical Behavior of Unsaturated Highly Expansive Clays." PhD thesis, Oxford University, UK, pp. 1 – 261.

Silva C. H. C., Porras, F. O., Fratta, D., & Macari, E, J. (2002). "Mechanical response of unsaturated particulate materials – A stiffness assessment study under controlled matric suction." Proceedings of IMECE2002 ASME International Mechanical Engineering Congress and Exposition, pp. 269 – 274.

Sivakumar, V., (1993) "A Critical State Framework for Unsaturated Soil." PhD Thesis, University of Sheffield, Sheffield, UK.

Skempton, A. W. (1960). "Effective stress in Soil, Concrete and Rocks." Proceedings of the Conference on Pore Water and Suction in Soils, pp. 04-16.

Stokoe, K. H. and Santamarina, J. C. (2000). State of the Art Report on "Seismic-Wave-Based Testing in Geotechnical Engineering". GeoEng Conference, Australia, pp. 1490- 1536.

Stokoe, K. H. I., Lee, S. H. H., and Knox, D. P. (1985). "Shear Moduli Measurements Under True Triaxial Stresses." Advances in the Art of Testing Soils Under Cyclic Conditions, ASCE, Detroit, MI, USA, pp. 166–185.

Thomann, T.G. and Hryciw, R.D. (1990). "Laboratory measurement of small strain shear modulus under K_0 conditions." Geotechnical Testing Journal, Vol. 13, pp. 97-105.

Vassallo, R., Mancuso, C., & Vinale, F. (2006). "Effects of stress – strain history on the initial shear stiffness of an unsaturated compacted silt." Geotechnical Special Publication No. 147, Unsaturated soils, Vol. 1, pp. 1145 – 1156.

Vinale, F., D'Onforio, A., Mancuso, C., Santicci de Magistris, F., and Tasuoka, F. (2001). "The pre-failure of soils as construction materials, Pre- failure deformation characteristics of Geomaterials." pp. 955-1007.

Viggiani, G. & Atkinson, J. H. (1995a). "Interpretation of bender element tests." Geotechnique, Vol. 45, No. 1, pp. 149 – 154.

Viggiani, G. & Atkinson, J. H. (1995b). "Stiffness of fine – grained soil at very small strain." Geotechnique, Vol. 45, No. 2, pp. 143 – 159.

Vucetic, M., and Dobry, R. (1991). "Effect of soils plasticity on cyclic response." Journal of Geotechnical Engineering, ASCE, Vol.117, No. 1, pp. 898-907.

Wheeler, S.J., Sharma, R.J. and Buisson, M.S.R. (2003). "Coupling of hydraulic hysteresis and stress-strain behavior in unsaturated soils." Geotechnique, Vol. 53, No. 1, pp. 41-54.

Wu, S., Gray, D. H., & Richart, F. E Jr. (1984). "Capillary effects on dynamic modulus of sands and silts." Journal for geotechnical and geo-environmental engineering, ASCE, Vol. 110, No. 9, pp. 1188 – 1203.

Yuen, Y. S. (2004). "Determination of shear wave velocity and anisotropic shear modulus of an unsaturated soil." M. Phil thesis, Hong Kong University of Science and Technology, pp. 01 – 194.

Zeng, Xiangwu., Ni, Bixian. (1998). "Measurement of G_0 under anisotropic loading condition using bender elements." Geotechnical Special Publication, Vol. 1, pp. 189-200.

Zeng, Xiangwu, Grolewski, Bartlomiej. (2005). "Measurement of G_{0max} and estimation of K_0 of saturated clay using bender elements in an oedometer." Geotechnical Testing Journal, Vol. 28, No. 3, pp. 264-274.

VITA

Ananth Bukkapatnam Tirumala was born in 1984, in Hyderabad, India. He completed his Bachelor's degree in Nedurumalli Balakrishna Reddy Institute of Science and Technology, Sri Venkateswara University, in April 2005. He worked as an Assistant Engineer for I. V. Reddy Construction Ltd. from May 2005 to June 2006 in Bangalore, India. He came to United States of America in July 2006, to pursue a master's degree in Geotechnical engineering in Louisiana State University. It is expected that he will fulfill the requirements for the Master of Science degree in Civil engineering in December 2008.